

The leptonic future of the Higgs

Gauthier Durieux,^a Christophe Grojean,^{a,b} ¹ Jiayin Gu,^{a,c} Kechen Wang^{a,c}

^a *DESY, Notkestraße 85, D-22607 Hamburg, Germany*

^b *Institut für Physik, Humboldt-Universität zu Berlin, D-12489 Berlin, Germany*

^c *Center for Future High Energy Physics, Institute of High Energy Physics, Chinese Academy of Sciences, Beijing 100049, China*

`gauthier.durieux@desy.de, christophe.grojean@desy.de, jiayin.gu@desy.de, kechen.wang@desy.de`

Abstract

Precision study of electroweak symmetry breaking strongly motivates the construction of a lepton collider with center-of-mass energy of at least 240 GeV. Besides Higgsstrahlung ($e^+e^- \rightarrow hZ$), such a collider would measure weak boson pair production ($e^+e^- \rightarrow WW$) with an astonishing precision. The weak-boson-fusion production process ($e^+e^- \rightarrow \nu\bar{\nu}h$) provides an increasingly powerful handle at higher center-of-mass energies. High energies also benefit the associated top-Higgs production ($e^+e^- \rightarrow t\bar{t}h$) that is crucial to constrain directly the top Yukawa coupling. The impact and complementarity of differential measurements, at different center-of-mass energies and for several beam polarization configurations, are studied in a global effective-field-theory framework. We define a *global determinant parameter* (GDP) which characterizes the overall strengthening of constraints independently of the choice of operator basis. The reach of the CEPC, CLIC, FCC-ee, and ILC designs is assessed.

¹On leave from Institució Catalana de Recerca i Estudis Avançats, 08010 Barcelona, Spain

Contents

1	Introduction	3
2	Effective-field-theory framework	5
3	Measurements and fit	8
3.1	Higgsstrahlung production	9
3.2	Higgs production through weak boson fusion	12
3.3	Higgs production in association with tops	13
3.4	Weak-boson pair production	14
3.5	Global fit and determinant parameter	16
4	Results	18
4.1	Impact of the various measurements	20
4.2	Impact of a 350 GeV run at circular colliders	22
4.3	Impact of beam polarization at linear colliders	23
4.4	Impact of systematic uncertainties in diboson production	24
4.5	Comparison with previous global analyses	26
5	Conclusions	26
A	Effective-field-theory parameter definitions	28
B	Measurement inputs	31
C	Additional figures	35
D	Numerical expressions for the observables	43
E	Numerical results of the global fit	46

1 Introduction

With the discovery of a scalar whose properties are compatible with that of the standard model (SM) Higgs boson, the first run of the LHC has found an essential ingredient for the deep understanding of matter and has revealed a fascinating and complex structure of the vacuum. As its second run is proceeding at an increased center-of-mass energy, no unambiguous sign of new physics (NP) has been found yet. Direct exploration of this energy frontier will continue for a couple of decades but a detailed understanding of electroweak symmetry breaking and the indirect search for NP via precision measurement would benefit from the cleaner environment of a lepton collider. An e^+e^- machine running at a center-of-mass energy of 240–250 GeV, close to the maximum of the $e^+e^- \rightarrow hZ$ Higgsstrahlung cross section would indeed determine the Higgs couplings with exquisite precision. Several proposals of such *Higgs factories* have been made, including the Circular Electron Positron Collider (CEPC) in China [1], the Future Circular Collider with e^+e^- (FCC-ee) at CERN, previously known as TLEP [2], and the International Linear Collider (ILC) in Japan [3]. The Compact Linear Collider (CLIC) at CERN [4] could also run at higher center-of-mass energies. The Higgs coupling measurements have been widely studied in the corresponding design studies through global fits in the so-called *kappa* framework [5].

As new physics is being constrained to lie further and further above the electroweak scale, the description of its effects at future lepton colliders seems to fall in a low-energy regime. Effective field theories (EFTs) therefore look like prime exploration tools [6–11]. Given that the parity of an operator dimension is that of $(\Delta B - \Delta L)/2$ [12], all operators conserving baryon and lepton numbers are of even dimension:

$$\mathcal{L}_{\text{EFT}} = \mathcal{L}_{\text{SM}} + \sum_i \frac{c_i^{(6)}}{\Lambda^2} \mathcal{O}_i^{(6)} + \sum_j \frac{c_j^{(8)}}{\Lambda^4} \mathcal{O}_j^{(8)} + \dots \quad (1.1)$$

where Λ is a mass scale and $c_i^{(d)}$ are the dimensionless coefficients of the $\mathcal{O}_i^{(d)}$ operators of canonical dimension d . The standard-model effective field theory (SMEFT) allows for a systematic exploration of the theory space in direct vicinity of the standard model, encoding established symmetry principles. As a genuine quantum field theory, its predictions are also perturbatively improvable. It therefore relies on much firmer theoretical bases than the *kappa* framework. While very helpful in illustrating the precision reach of Higgs measurements, the latter can in particular miss interactions of Lorentz structure different from that of the standard model, or correlations deriving from gauge invariance, notably between Higgs couplings to different gauge bosons.

Many effective-field-theory studies have been performed, for Higgs measurements at LHC [13–17], electroweak (EW) precision observables at LEP [18–22], diboson measurements at both LEP [23] and LHC [24, 25], or the combination of measurements in several sectors [26, 27]. Among the studies performed in the context of future Higgs factories [28–36], many estimated constraints on individual dimension-six operators. A challenge related to the consistent use of the EFT framework is indeed the simultaneous inclusion

of all operators up to a given dimension. It is required for this approach to retain its power and generality. As a result, various observables have to be combined to constrain efficiently all directions of the multidimensional space of effective-operator coefficients. The first few measurements included bring the more significant improvements by lifting large approximate degeneracies. Besides Higgsstrahlung production and decay rates in different channels, angular distributions contain additional valuable information [29, 31]. Our knowledge about differential distributions could also be exploited more extensively through statistically optimal observables [37, 38]. Higgs production through weak-boson fusion provides complementary information of increasing relevance at higher center-of-mass energies. Direct constraints on the top Yukawa coupling can moreover only be obtained through Higgs production in association with a pair of tops. Measurements at $\sqrt{s} = 350$ GeV and above can thus be very helpful. As the sensitivities to operator coefficients can vary with \sqrt{s} , these higher-energy runs would also constrain different directions of the parameter space and therefore resolve degeneracies. Beam polarization, more easily implemented at linear colliders, could be similarly helpful. Finally, the Higgs and anomalous triple gauge couplings (aTGCs) are related in a gauge-invariant EFT, and a subset of operators relevant for Higgs physics can be efficiently bounded through diboson production $e^+e^- \rightarrow WW$ [17, 23].

We parametrize deviations from the standard-model in the processes enumerated above through dimension-six operators, in the so-called Higgs basis [39]. Translation to other bases is however straightforward. Our assumption of perfectly standard-model-like electroweak precision measurements is more easily implemented in that framework. No deviation in the gauge-boson couplings to fermions, or W mass is permitted. Given the poor sensitivity expected for the Yukawa couplings of lighter fermion, we only allow for modifications of the (flavor-conserving) muon, tau, charm, bottom, and top ones. Neither CP-violating, nor fermion dipole operators are considered. The potential impact of these assumptions on our results is carefully discussed in the text. A global effective-field-theory analysis is then performed, in a twelve-dimensional parameter space, assuming that measurements coincide with their SM predictions. Prospects for the different machines are discussed in view of their respective design and run plan.

The rest of this paper is organized as follows. In [Section 2](#), we lay down the EFT framework used. In [Section 3](#), we detail the observables included in our study. The results of the global fits are shown in [Section 4](#). The reach of the different colliders is summarized in [Fig. 7](#). Our conclusions are drawn in [Section 5](#). Further details are provided in the appendix. We define our twelve effective-field-theory parameters and provide their expressions in the SILH' basis in [Appendix A](#). Additional information about the measurement inputs is provided in [Appendix B](#). Supplementary figures and results are available in [Appendix C](#). In [Appendix D](#), we provide numerical expressions for the observables used in terms of our twelve effective-field-theory parameters. Finally, the numerical results of the global fits are tabulated in [Appendix E](#). They could be used to set limits on specific models while accounting for the correlations in the full twelve-dimensional parameter space.

2 Effective-field-theory framework

A global effective-field-theory treatment of any process requires to consider simultaneously all contributing operators appearing in a complete basis, up to a given dimension. Assuming baryon and lepton number conservations, we restrict ourselves to dimension-six operators. As mentioned in the introduction, we would like to model the following processes:

- Higgsstrahlung production: $e^+e^- \rightarrow hZ$ (rates and distributions), followed by Higgs decays in various channels,
- Higgs production through weak-boson fusion: $e^+e^- \rightarrow \nu\bar{\nu}h$,
- Higgs production in association with top quarks: $e^+e^- \rightarrow t\bar{t}h$,
- weak-boson pair production: $e^+e^- \rightarrow WW$ (rate and distributions).

Several combinations of operators affecting these processes are however well constrained by other measurements. As discussed in [Section 3.4](#), electroweak precision observables could be constrained to a sufficient level, although this remains to be established explicitly. At leading order, CP-violating operators give no linear contribution to the Higgs rates but could manifest themselves in angular asymmetries [[29](#), [31](#)]. They could moreover be well constrained by dedicated searches. Under restrictive assumptions, indirect constraints arising from EDM experiments [[40–42](#)] for instance render Higgs CP-violating asymmetries inaccessible at future colliders [[31](#)], even though some room may be left in the CP violating Yukawa of the charm and bottom quarks for which the direct and indirect bounds are not that restrictive [[43](#)]. It is also possible for CP violating Yukawa couplings of heavy flavor leptons to evade the constraints from EDM experiments which could be probed in Higgs decays [[44](#)]. As a first working hypothesis, we thus assume electroweak and CP-violating observables are perfectly constrained to be standard-model like.

Throughout this paper, we only retain the interferences of effective-field-theory amplitudes with standard-model ones. The squares of amplitudes featuring a dimension-six operator insertion are discarded. They are formally of the same c^2/Λ^4 order as the interferences of dimension-eight operators with standard-model amplitudes. The relative importance of these two kinds of c^2/Λ^4 contributions can however not be determined without assuming a definite power counting or referring to a specific model. Nevertheless, thanks to the high precision to which most observables are measured at lepton colliders that collect large amount of integrated luminosity in clean environments, we generically expect the discarded terms to have small impact on our results. The percent-level measurement of an observable of schematic

$$\frac{O}{O_{\text{SM}}} = 1 + \mathcal{O}(1)\frac{cE^2}{\Lambda^2} + \mathcal{O}(1)\left(\frac{cE^2}{\Lambda^2}\right)^2$$

effective-field-theory dependence (where E is a typical energy scale) will for instance constrain $c E^2/\Lambda^2$ at the percent level. The quadratic term then only induces a relative percent-level correction to this limit. In specific cases, the interference of dimension-six operators with standard-model amplitudes can however suffer accidental suppressions. This could invalidate the naïve hierarchy above between linear and quadratic terms. Helicity selection rules [45] can for instance cause significant suppressions of the linear contribution compared to the quadratic one, at energies higher than electroweak mass scales. If the standard model and dimension-six operators give rise to amplitudes with electroweak bosons of different helicities, their interference is expected to scale as cm_V^2/Λ^2 . A measurement of O/O_{SM} with precision x would still imply a limit of order x on cm_V^2/Λ^2 at low energies but this bound would receive corrections scaling as $x E^4/m_V^4$ for increasing E . Given m_V of order 100 GeV, only measurements of 10^{-2} , 10^{-3} , 10^{-4} , 10^{-5} and 10^{-6} precisions at least are roughly expected to be dominated by linear effective-field-theory contributions at 250, 500, 1000, 1400 and 3000 GeV energies, respectively. We will comment further on accidental suppressions and on their possible impact on our results in [Section 4](#). Light fermion dipole operators also have interferences with standard-model amplitudes that suffer drastic mass suppressions. As a consequence, their dominant effects arise at the c^2/Λ^4 level. We however leave the study of this family of operators for future work.

Under the above assumptions, together with flavor universality, it was shown that there are 10 independent combinations of operators that contribute to Higgs (excluding its self coupling) and TGC measurements [13, 14, 16, 23].¹ We however lift the flavor universality requirement and treat separately the top, charm, bottom, tau, and muon Yukawa couplings. No flavor violation is allowed and we refer to Refs. [46–48] for studies of the possible means to probe the light-fermion Yukawas at present and future experiments. In total, 12 degrees of freedom are thus considered. While all non-redundant basis are equivalent, we find the Higgs basis [39] particularly convenient. It is defined in the broken electroweak phase and therefore closely related to experimental observables. Distinguishing the operators contributing to electroweak precision measurements from the ones of Higgs and TGC measurements is also straightforward in this basis. The parameters we use are:

$$\delta c_Z, \quad c_{ZZ}, \quad c_{Z\Box}, \quad c_{\gamma\gamma}, \quad c_{Z\gamma}, \quad c_{gg}, \quad \delta y_t, \quad \delta y_c, \quad \delta y_b, \quad \delta y_\tau, \quad \delta y_\mu, \quad \lambda_Z. \quad (2.1)$$

Their exact definitions as well as a correspondence map to the SILH' basis of gauge-invariant dimension-six operators can be found in [Appendix A](#). The numerical expressions of the various observables we use as functions of these parameters are given in [Appendix D](#).

Compared to the widely-used *kappa* framework, an important feature of this effective field theory is the appearance of Higgs couplings with Lorentz structures differing from SM ones. In addition to $\delta c_Z h Z_\mu Z^\mu$ which modifies an existing SM coupling, the

¹Refs. [26, 32, 35] additionally set lepton and down-type Yukawa couplings equal while Ref. [17] focuses on third-generation fermions instead of assuming flavor universality.

$c_{ZZ} hZ_{\mu\nu}Z^{\mu\nu}$ and $c_{Z\Box} hZ_{\mu}\partial_{\nu}Z^{\mu\nu}$ interactions are for instance also generated by gauge-invariant dimension-six operators. The $e^+e^- \rightarrow hZ$ rate, at a given center-of-mass energy and for a fixed beam polarization, depends on one combination of these parameters. Runs at various energies, with different beam polarizations, as well as additional measurements are therefore crucial to constrain all other orthogonal directions. Measurements at higher center-of-mass energies have an enhanced sensitivity to c_{ZZ} and $c_{Z\Box}$. Angular asymmetries in $e^+e^- \rightarrow hZ$, weak-boson-fusion production rate, weak-boson pair production, or the $h \rightarrow ZZ^*$ and $h \rightarrow WW^*$ decays, each play a role. The measurement of the $h \rightarrow Z\gamma$ decay is crucial too. The $c_{Z\gamma}$ coupling which contributes to the Higgsstrahlung process otherwise remains loosely constrained and weakens the whole fit.

The treatment of the $h \rightarrow gg$, $\gamma\gamma$, and $Z\gamma$ decays requires some special attention. Given that they are loop-level generated in the standard model, one may wish to include their loop-level dependence in effective parameters like δy_t , δy_b , δc_W which rescale standard-model interactions, or c_{ZZ} , $c_{Z\Box}$, etc. which do not. Complete effective-field-theory results at that order are however not currently available for the above processes (see Ref. [49] for the treatment of $h \rightarrow \gamma\gamma$). The computation of next-to-leading-order effective-field-theory contributions to processes that are not loop-level generated in the standard model would also be needed to ensure a consistent global treatment. Misleading results can otherwise be obtained. Let us illustrate this point with the dependence of the $h \rightarrow \gamma\gamma$ partial width on $c_{\gamma\gamma}$ and δy_t , at tree- and loop-level, respectively. The Higgsstrahlung, weak-boson fusion, and weak-boson pair production processes also depend at tree level on $c_{\gamma\gamma}$ and receive loop corrections proportional to δy_t . A combination of these two parameters similar to the one entering in the $h \rightarrow \gamma\gamma$ partial width may moreover be expected. Including the dependence of this partial width on δy_t , but not that of the $e^+e^- \rightarrow hZ$, $e^+e^- \rightarrow \nu\bar{\nu}h$, and $e^+e^- \rightarrow WW$ cross sections, one would artificially render their constraints orthogonal. Tight bounds on δy_t would then be obtained. Consistently including all one-loop dependences on these parameters might however still leave a combination of $c_{\gamma\gamma}$ and δy_t at least nearly unconstrained. To avoid such a pitfall, we choose not to include any loop-level dependence on effective-field-theory parameters in the $h \rightarrow \gamma\gamma$ and $Z\gamma$ partial widths. Once direct constraints on the top Yukawa coupling (from the LHC or from $e^+e^- \rightarrow t\bar{t}h$) are included, we however checked that including the whole loop dependence of the $h \rightarrow \gamma\gamma$ branching fraction has only marginal effects on our results.² For our purpose, it is on the contrary safe to account for the loop-level δy_t and δy_b dependences of the $h \rightarrow gg$ partial width. It remains to be examined whether the loop-level dependence on δy_t in processes measured at lepton collider, below the $t\bar{t}h$ threshold, could serve to improve on the high-luminosity LHC constraints. A similar question, asked for the trilinear Higgs coupling [51] could be further investigated.

Absorbing also, for convenience, a standard-model normalization factor into barred

²We used the numerical expressions derived from the results of Ref. [49] in the appendix of Ref. [50].

effective parameters, we thus obtain:

$$\frac{\Gamma_{\gamma\gamma}}{\Gamma_{\gamma\gamma}^{\text{SM}}} \simeq 1 - 2\bar{c}_{\gamma\gamma}, \quad \frac{\Gamma_{Z\gamma}}{\Gamma_{Z\gamma}^{\text{SM}}} \simeq 1 - 2\bar{c}_{Z\gamma}, \quad (2.2)$$

and

$$\frac{\Gamma_{gg}}{\Gamma_{gg}^{\text{SM}}} \simeq 1 + 2\bar{c}_{gg}^{\text{eff}} \simeq 1 + 2\bar{c}_{gg} + 2.10\delta y_t - 0.10\delta y_b, \quad (2.3)$$

at the linear order. Compared to the standard Higgs-basis effective parameters, our normalization is the following:

$$\bar{c}_{\gamma\gamma} \simeq \frac{c_{\gamma\gamma}}{8.3 \times 10^{-2}}, \quad \bar{c}_{Z\gamma} \simeq \frac{c_{Z\gamma}}{5.9 \times 10^{-2}}, \quad \bar{c}_{gg} \simeq \frac{c_{gg}}{8.3 \times 10^{-3}}. \quad (2.4)$$

We will sometimes display results in terms of the $\bar{c}_{gg}^{\text{eff}}$ parameter that is directly probed by the $h \rightarrow gg$ branching fraction. It is particularly informative to do so when c_{gg} and δy_t are only poorly constrained individually.

Measurement of the $h \rightarrow ZZ^*$ rate relies on its fermionic decay products and has some sensitivity on $c_{\gamma\gamma}$ and $c_{Z\gamma}$, in addition to δc_Z , c_{ZZ} and $c_{Z\Box}$. Higgs decays to off-shell photons can indeed produce the same final state. Each fermionic decay channel actually has a somewhat different sensitivity which depends strongly on the invariant mass of fermion pairs. Loosened cuts would provide increased sensitivities to $c_{\gamma\gamma}$ and $c_{Z\gamma}$ [52].³ For simplicity, we however neglect the contributions of those two effective-field-theory parameters to $h \rightarrow ZZ^*$. Standard invariant mass cuts together with the constraints on $c_{\gamma\gamma}$ and $c_{Z\gamma}$ arising from the direct measurements of $h \rightarrow Z\gamma$ and $h \rightarrow \gamma\gamma$ decays should be sufficient to limit the impact of this approximation on our results.

The standard-model effective field theory we use specifically assumes the absence of new states below the electroweak scale. It does therefore not account for possible invisible decays of the Higgs. The corresponding branching fraction would nevertheless be significantly constrained at future lepton colliders. An integrated luminosity of 5 ab^{-1} collected at 240 GeV would for instance bound $\sigma(hZ) \times \text{BR}(h \rightarrow \text{inv})$ to be smaller than 0.28% of $\sigma(hZ)$ at the 95% CL [1]. Other exotic Higgs decays not modeled in a SMEFT framework would also be constrained very well at future lepton colliders [54]. We do therefore not expect an effective field theory modified to include such decays to lead to results widely different from the ones we obtain.

3 Measurements and fit

To the best of our knowledge, the most updated run plans of each machine are the following:

³See also Ref. [53] for a recent EFT study of the Higgs decay into four charged leptons exploiting both the rates and kinematic distributions.

- According to its preCDR, the CEPC would collect 5 ab^{-1} of integrated luminosity at 240 GeV. Recently, the reference circumference of its tunnel has been fixed to 100 km [55]. A run at 350 GeV could therefore be envisioned. The luminosity to expect at that center-of-mass energy however depends on the machine design and is currently unknown. To study the impact of the measurements at 350 GeV, we take a conservative benchmark value of 200 fb^{-1} and explore a larger range in Section 4.
- The CDR of the FCC-ee project is expected by the year 2018 [56] and will supersede the TLEP white paper [2] that still contains the most recent results on Higgs physics. The latter document, we rely on, assumes that 10 ab^{-1} of data would be collected at 240 GeV and 2.6 ab^{-1} at 350 GeV.
- Recent ILC documents suggest that, with a luminosity upgrade, it could collect 2 ab^{-1} at 250 GeV, 200 fb^{-1} at 350 GeV, and 4 ab^{-1} at 500 GeV [57, 58]. This significantly extends the plans presented in its TDR [3]. The updated estimations are adopted in our study. The ILC could also run with longitudinally polarized beams. We follow Refs. [3, 58] and assume that a maximum polarization of $\pm 80\%$ ($\pm 30\%$) can be achieved for the incoming electron (positron). While collecting 1 ab^{-1} of integrated luminosity at a center-of-mass energy of 1 TeV, with $P(e^-, e^+) = (-0.8, +0.2)$ polarization, is also considered in the TDR [3], we follow Ref. [57, 58] and do not take such a run into account. Nevertheless, results including the 1 TeV measurements of precision quoted in Ref. [59] are shown in Appendix C.
- Recent Ref. [4] proposed that CLIC would collect 100 fb^{-1} at the top threshold, 500 fb^{-1} at 380 GeV, 1.5 ab^{-1} at 1.5 TeV, and 3 ab^{-1} at 3 TeV. The more specific study of Higgs measurements of Ref. [60] however assumed 500 fb^{-1} at 350 GeV, 1.5 ab^{-1} at 1.4 TeV and 2 ab^{-1} at 3 TeV. We follow the latter plan in order to make use of its estimations. While the implementation of beam polarization is also likely at CLIC, we follow again Ref. [60] and assume unpolarized beams.

In the rest of this section, we summarize the important aspects of each of the measurements we take into account. We detail the assumptions made in the many cases where necessary information is not provided in the literature. The numerical inputs we use are given in Appendix B.

3.1 Higgsstrahlung production

Rate measurements

The Higgsstrahlung process (see Fig. 1) dominates the Higgs production modes at lepton colliders below center-of-mass energies of about 450 GeV where weak-boson fusion takes over. Its cross section is maximized around 250 GeV but bremsstrahlung makes it more advantageous for circular colliders to run at 240 GeV. At this energy, an integrated luminosity of 5 ab^{-1} would yield about 1.06×10^6 Higgses. At 250 GeV, 2 ab^{-1} of data collected

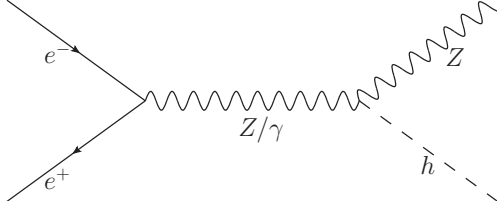


Figure 1: Leading-order contribution to the Higgsstrahlung process, $e^+e^- \rightarrow hZ$.

with $P(e^-, e^+) = (-0.8, +0.3)$ beam polarization would contain approximately 6.4×10^5 Higgses. The latter polarization configuration maximizes the $e^+e^- \rightarrow hZ$ cross section. The recoil mass of the Z gives access to the inclusive $e^+e^- \rightarrow hZ$ rate independently of the exclusive Higgs decay channels measurements. The Higgsstrahlung process can also be measured at higher center-of-mass energies. Despite the smaller cross sections, this allows to probe different combinations of EFT parameters and is thus helpful for resolving (approximate) degeneracies among them. The estimated measurement precisions at each collider and at different energies are shown in Table 2, 3 and 4 of Appendix B, where further details are also provided.

A few important comments are in order. As mentioned in Section 2, the measurement of the rare $h \rightarrow Z\gamma$ decay, while not very constraining for the SM $hZ\gamma$ coupling, could be very important to resolve the degeneracies of EFT parameters in the production processes. Therefore, while the estimation of this measurement is not available for the FCC-ee and ILC, we scale the precision estimated for the CEPC, assuming the dominance of statistical uncertainties. Some care must also be taken to avoid potential double counting between the $e^+e^- \rightarrow hZ$, $Z \rightarrow \nu\bar{\nu}$, $h \rightarrow b\bar{b}$ process and the weak-boson fusion $e^+e^- \rightarrow \nu\bar{\nu}h$, $h \rightarrow b\bar{b}$, which yield the same final state. This is further discussed in Section 3.2 and Appendix B. Note also that the interferences between s -channel Z and photon amplitudes are accidentally suppressed by a factor of $1 - 4\sin^2\theta_W \simeq 0.06$ in the total unpolarized cross section. This factor arises from the sum of the left- and right-handed couplings of the electron to the Z , $\frac{e}{2s_W c_W}(-1+2s_W^2)$ and $\frac{e}{2s_W c_W}(2s_W^2)$, respectively. Beam polarization thus significantly affects the sensitivity of the Higgsstrahlung rate to operators contributing to the $hZ\gamma$ vertex.⁴ Numerical expressions in the Higgs basis are provided in Eq. (D.1). Introducing $c_{\gamma\Box}$ defined in Eq. (A.3) and contributing for an off-shell photon however renders this effect more transparent. For $P(e^-, e^+) = (0, 0)$, $(-0.8, +0.3)$, $(+0.8, -0.3)$ polarization configurations at $\sqrt{s} = 250$ GeV, we for instance obtain:

$$\frac{\sigma_{hZ}}{\sigma_{hZ}^{\text{SM}}}\bigg|_{250 \text{ GeV}}^{P=\begin{pmatrix} (0, 0) \\ (-0.8, +0.3) \\ (+0.8, -0.3) \end{pmatrix}} \simeq 1 + 2\delta c_Z + 1.6 c_{ZZ} + 3.5 c_{Z\Box} + \begin{pmatrix} 0.060 \\ 0.82 \\ -0.89 \end{pmatrix} c_{Z\gamma} + \begin{pmatrix} 0.16 \\ 2.2 \\ -2.3 \end{pmatrix} c_{\gamma\Box}. \quad (3.1)$$

An increase in the sensitivity magnitude of more than an order of magnitude is brought

⁴We thank Michael Peskin for helping us understand this interesting phenomena.

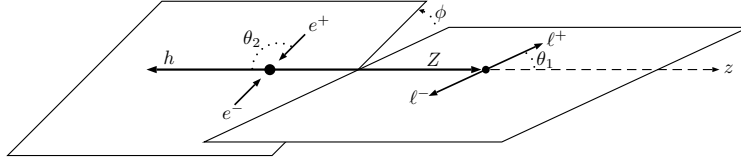


Figure 2: Definition of the $\Omega = \{\theta_1, \theta_2, \phi\}$ angles in a $e^+e^- \rightarrow hZ$ event (taken from Ref. [31]). Note the two polar angles are respectively defined in the center-of-mass and Z restframes.

by beam polarization. Reversing the polarization also flips the sign of the $c_{Z\gamma}$ and $c_{\gamma\Box}$ prefactors, given the opposite signs of the left- and right-handed couplings of the Z to electrons.

Angular asymmetries

Three angles and two invariant masses fully characterize the differential distribution of the $e^+e^- \rightarrow hZ \rightarrow hf\bar{f}$ process (see Fig. 2). It naturally provides information complementary to that of the total rate alone. The effective-field-theory contributions to the angular distributions have been thoroughly studied in Ref. [29]. At tree level and linear order in the effective-field-theory parameters, they can all be captured through the following asymmetries:

$$\begin{aligned}
\mathcal{A}_{\theta_1} &= \frac{1}{\sigma} \int d\Omega \operatorname{sgn}\{\cos(2\theta_1)\} \frac{d\sigma}{d\Omega}, \\
\mathcal{A}_{\phi}^{(1)} &= \frac{1}{\sigma} \int d\Omega \operatorname{sgn}\{\sin\phi\} \frac{d\sigma}{d\Omega}, \\
\mathcal{A}_{\phi}^{(2)} &= \frac{1}{\sigma} \int d\Omega \operatorname{sgn}\{\sin(2\phi)\} \frac{d\sigma}{d\Omega}, \\
\mathcal{A}_{\phi}^{(3)} &= \frac{1}{\sigma} \int d\Omega \operatorname{sgn}\{\cos\phi\} \frac{d\sigma}{d\Omega}, \\
\mathcal{A}_{\phi}^{(4)} &= \frac{1}{\sigma} \int d\Omega \operatorname{sgn}\{\cos(2\phi)\} \frac{d\sigma}{d\Omega}, \\
\mathcal{A}_{c\theta_1, c\theta_2} &= \frac{1}{\sigma} \int d\Omega \operatorname{sgn}\{\cos\theta_1 \cos\theta_2\} \frac{d\sigma}{d\Omega},
\end{aligned} \tag{3.2}$$

where $\Omega = \{\theta_1, \theta_2, \phi\}$ and the sgn function gives the sign of its argument. Among these asymmetries, $\mathcal{A}_{\phi}^{(1)}$ and $\mathcal{A}_{\phi}^{(2)}$ are sensitive to CP-violating parameters (or absorptive parts of amplitude), while \mathcal{A}_{θ_1} and $\mathcal{A}_{\phi}^{(4)}$ depend on the same combination of operator coefficients. In the absence of CP violation, the angular observables therefore provide three independent constraints on effective-field-theory parameters. The corresponding Higgs-basis expressions are provided in Appendix D.

A phenomenological study of these angular asymmetries at circular e^+e^- colliders has been performed in Ref. [31]. In particular, it was shown that the uncertainties on

their determination is statistics dominated for leptonic Z decays. The absolute statistical uncertainty (one standard deviation) on each asymmetry \mathcal{A} measured with N events is given by [31]

$$\sigma_{\mathcal{A}} = \sqrt{\frac{1 - \mathcal{A}^2}{N}} \approx \frac{1}{\sqrt{N}}. \quad (3.3)$$

Following Ref. [31], we use only the events with Higgs decays to bottom quarks ($e^+e^- \rightarrow hZ$, $Z \rightarrow \ell^+\ell^-$, $h \rightarrow b\bar{b}$) which has negligible backgrounds. Reference [31] refers to a preliminary version of the CEPC preCDR which suggests the signal selection efficiency of this channel at 240 GeV is around 54%. For simplicity, we assume a universal efficiency of 60% for the event selection of this channel at all energies for the angular asymmetry analysis. For the CEPC, with 5 ab^{-1} collected at 240 GeV, this constitutes a subsample of approximately 2.7×10^4 Higgsstrahlung events. For the ILC, the effects of beam polarizations on the asymmetries is taken into account. No systematic uncertainty is included. We however expect statistical uncertainties to be dominant given the fairly rare but clean Z decay to leptons.

3.2 Higgs production through weak boson fusion

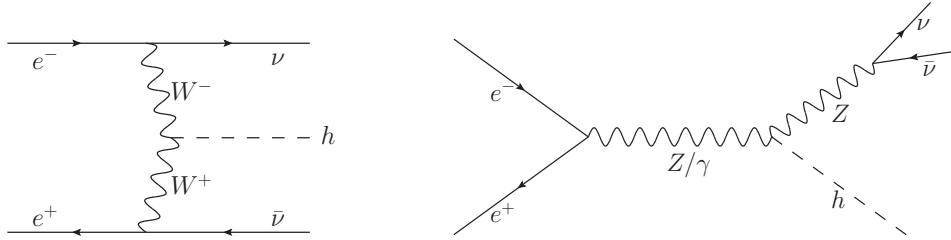


Figure 3: Two contributions to the $e^+e^- \rightarrow \nu\bar{\nu}h$ process: weak-boson fusion (left), and $e^+e^- \rightarrow hZ, Z \rightarrow \nu\bar{\nu}$ (right).

The Higgs couplings to W , Z bosons, and photons are related by $SU(2)_L$ gauge invariance. As such, the measurement of the weak-boson fusion process, first considered in e^+e^- colliders in Ref. [61], is complementary to that of the Higgsstrahlung process. So, a combination of the two measurements can efficiently resolve the degeneracy among the EFT parameters that contribute to the production processes. The weak-boson fusion cross section grows with energy, so that it is better measured at a center-of-mass energy of 350 GeV or above. Nevertheless, the measurement at 240 GeV can still provide important information, especially if runs at higher energies are not performed.

Importantly, Higgsstrahlung with Z decay to neutrinos ($e^+e^- \rightarrow hZ, Z \rightarrow \nu\bar{\nu}$) yields the same final state as weak-boson fusion (see Fig. 3) and has a rate about six times larger at a center-of-mass energy of 240 GeV (without beam polarization). At this center-of-mass energy the missing mass distributions for both processes moreover peak at similar energies (see Fig. 3.16 on page 75 of Ref. [1]). Isolating the weak-boson fusion contribution

is therefore difficult. For the CEPC and FCC-ee at 240 GeV, we therefore consider an inclusive $e^+e^- \rightarrow \nu\bar{\nu}h$ sample to which the two processes contribute, and only use the $h \rightarrow b\bar{b}$ channel for which the precision on the $e^+e^- \rightarrow \nu\bar{\nu}h$ rate measurement is reported in the literature. We neglect the contributions of the weak-boson fusion in the other Higgs decay channels of $e^+e^- \rightarrow hZ$, $Z \rightarrow \nu\bar{\nu}$. For the ILC, Ref. [59] states that a χ^2 fit of the recoil mass distribution is used to separate the weak-boson-fusion and the Higgsstrahlung processes. We thus consider that the precision on $\sigma(e^+e^- \rightarrow \nu\bar{\nu}h) \times \text{BR}(h \rightarrow b\bar{b})$ quoted in Ref. [58] applies directly to the weak-boson fusion contribution. Both processes reach equal rates at a center-of-mass energy close to 350 GeV (without beam polarization). At this and higher energies, we thus assume that their distinct recoil-mass distributions are sufficient to efficiently separate them. More details on the treatment of this measurement can be found in [Appendix B](#).

3.3 Higgs production in association with tops

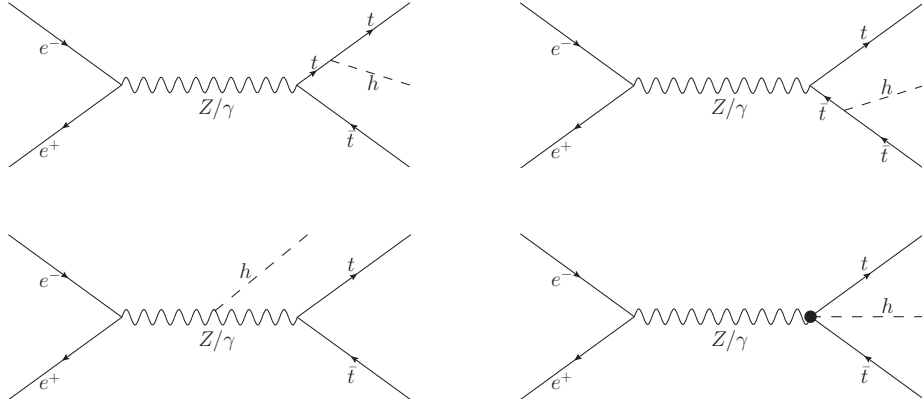


Figure 4: Leading-order diagrams for the $e^+e^- \rightarrow t\bar{t}h$ process. In the SM, the dominant contributions are the ones involving the top Yukawa coupling. Other EFT contributions (including that of four-fermion operators, not depicted) should be well constrained by other measurements.

The $e^+e^- \rightarrow t\bar{t}h$ production of a Higgs boson in association with top quarks (see [Fig. 4](#)) requires a large center-of-mass energy which is only achieved at a linear collider. A 10% precision on $\sigma(t\bar{t}h) \times \text{BR}(h \rightarrow b\bar{b})$ could be achieved with 4 ab^{-1} of ILC data collected at $\sqrt{s} = 500 \text{ GeV}$ (scaled from 28% of the 500 fb^{-1} result in Ref. [58]). At CLIC, 1.5 ab^{-1} of 1.4 TeV data should yield an 8.4% precision [60]. In the SM, the dominant contributions to this process involve a top Yukawa coupling. The radiation of a Higgs from the s -channel Z boson is comparatively negligible [3]. In the effective field theory, we only include modifications of the top Yukawa coupling. Other contributions should be sufficiently constrained by the measurement of top pair production and other processes. Neither the four-point $Zhtt$ interaction depicted on [Fig. 4](#) (bottom-right), nor four-fermion operator contributions are thus accounted for here. This channel could also be used to

establish the CP properties of the Higgs boson [62], which we simply assumed to be a 0^+ state throughout our analysis.

3.4 Weak-boson pair production

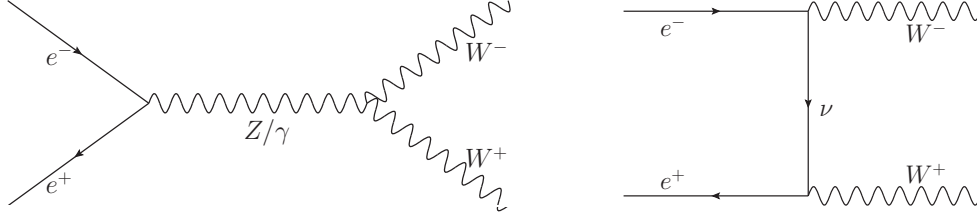


Figure 5: Leading-order diagrams contributing to $e^+e^- \rightarrow WW$. The s -channel diagram on the left with an intermediate Z or photon involves a triple gauge coupling.

The diagrams contributing to the $e^+e^- \rightarrow WW$ process, at leading order, are depicted in Fig. 5. The s -channel diagrams with an intermediate Z or photon involve triple gauge couplings. Considering CP-even dimension-six operators only, the aTGCs are traditionally parameterized using $\delta g_{1,Z}$, $\delta \kappa_\gamma$ and λ_Z [63, 64], defined in Eq. (A.5). Among them, $\delta g_{1,Z}$ and $\delta \kappa_\gamma$ are generated by effective operators that also contribute to Higgs observables. As pointed out in Ref. [23], this leads to an interesting interplay between Higgs and TGC measurements.

Triple gauge couplings have been measured thoroughly at LEP2 [65]. Various studies of future lepton colliders’ reach have also been carried out [66–71]. At future circular colliders, most of the W pairs are likely to be produced at 240 GeV, as a byproduct of the Higgs measurement run which requires large luminosities. At this energy, the $e^+e^- \rightarrow WW$ cross section is approximately two orders of magnitude larger than that of $e^+e^- \rightarrow hZ$. With 5 ab^{-1} , the CEPC would thus produce about 9×10^7 $e^+e^- \rightarrow WW$ events, thereby improving significantly our knowledge of TGCs. A run at 350 GeV, probing a different combination, could bring further improvement on the constraints. Longitudinal beam polarization is also very helpful in probing the aTGCs. With 500 fb^{-1} collected at 500 GeV and equally shared between four $P(e^-, e^+) = (\pm 80\%, \pm 30\%)$ beam polarization configurations, the ILC could constrain the three TGCs to the 10^{-4} level [68]. Note the runs with $++$ and $--$ polarizations are mostly meant to provide a simultaneous and sufficiently accurate polarization magnitude measurement. Comparable results can be expected for more realistic repartitions of the luminosities [69].

For the CEPC and FCC-ee prospects, we follow Ref. [71] which exploited kinematic distributions in the $e^+e^- \rightarrow WW \rightarrow 4f$ process. Five angles can be reconstructed in each such event: the polar angle between the incoming e^- and the outgoing W^- , and two angles specifying the kinematics of each W decay products. When both W s decay leptonically, the W mass constraints allow to fully reconstruct the kinematics up to a fourfold ambiguity at most. Here, we make the optimistic assumption that the correct

solution is always found. In the hadronic W decays, one can not discriminate between the quark and antiquark. The angular distributions of the W decay products are thus *folded*. We divide the differential distributions of each angle into 20 bins (10 in folded distributions). Uncorrelated Poisson distributions are assumed in each bin and their χ^2 are summed over. The total χ^2 is constructed by summing over the χ^2 of all the angular distributions of all decay channels. The statistical correlation between angular distributions is neglected.

Given the huge statistics that would be collected, and although they were neglected in Ref. [71], the systematic uncertainties could play an important role. Theoretical uncertainties could also become limiting. At the moment, there is however no dedicated experimental study of TGC measurements at future circular colliders. We therefore introduce a benchmark systematic uncertainty of 1% in each bin of the differential distributions. This guess is probably too conservative compared to few 10^{-4} systematic uncertainties on the $\delta g_{1,Z}$, $\delta \kappa_\gamma$, and λ_Z TGC parameters recently estimated by the ILC collaboration [72]. We therefore examine the impact of variation of this value in Section 4 and also provide constraints obtained by assuming no deviation on the TGC from their standard-model values.

For the prospects of the full ILC program, we use the one-sigma statistical uncertainties obtained in Ref. [68] ($\Delta\delta g_{1,Z} = 6.1 \times 10^{-4}$, $\Delta\delta \kappa_\gamma = 6.4 \times 10^{-4}$ and $\Delta\lambda_Z = 7.2 \times 10^{-4}$), together with their correlations shown in Table 7 of Appendix B. We do however not scale these numbers to higher luminosities, as systematic uncertainties are likely to become important. The current estimates by the ILC collaboration for systematics uncertainties are of a few 10^{-4} [72]. When focusing on the 250 and 350 GeV runs of the ILC, we use the strategy described above for the CEPC instead. As a dedicated experimental study of TGC measurements at CLIC is also missing,⁵ we assume a precision similar to the ILC one can be reached there. It should be noted, however, that the 1.4 and 3 TeV runs at CLIC could potentially provide even stronger constraints on the aTGCs due to the increase of sensitivities with energy [35].

Another important issue raised by the significant improvement in the $e^+e^- \rightarrow WW \rightarrow 4f$ measurement precision concerns the uncertainty on electroweak precision observables. In the extraction of the constraints on aTGCs, one usually makes the *TGC dominance assumption* and neglects the impact of new physics on all other parameters. At LEP, this was justified given the better precision of Z -pole and W -mass measurements compared to that of W pair production. In this work, we also assume that runs at lower energies will give us sufficient control on such effects. Exploiting diboson data could also be an alternative if runs at lower energies are not performed. Further investigations are

⁵ For CLIC at 3 TeV and an integrated luminosity of 1 ab^{-1} , Ref. [67] bases itself on Ref. [66] which derived individual constraints and quotes $\Delta\delta \kappa_\gamma = 0.9 \times 10^{-4}$, $\Delta\lambda_Z = 1.3 \times 10^{-4}$ constraints (we thank Philipp Roloff for pointing out this reference). These results are however insufficient to serve as input for our global analysis. A phenomenological study for CLIC based on total $e^+e^- \rightarrow WW$ rates only was also performed in Ref. [35]. The results in Section 3.2 and Eq. (4.2) there imply individual constraints rescaled for 1 ab^{-1} that are less than a factor of two better than that of Ref. [67].

required in this direction. The W mass can be measured very well at a Higgs factory by reconstructing the W decay products in the $e^+e^- \rightarrow WW$ process. To leading order, the aTGCs affect the differential distributions of $e^+e^- \rightarrow WW$, but not the W invariant mass. The two measurements are thus approximatively independent. A precision of 3 MeV could be achieved at the CEPC with this method [1]. A dedicated threshold scan at center-of-mass energies of 160–170 GeV could also be performed. As such, it is reasonable to assume the W mass will be sufficiently well constrained at future e^+e^- colliders. The corrections to gauge-boson propagators and fermion gauge couplings could however have a non-negligible impact on the determination of triple gauge couplings, especially without a future Z factory to improve their constraints.⁶ While the CEPC and FCC-ee could perform a run at the Z pole, the interest of such a Z -pole run at the ILC and CLIC is still under investigation. Notably, the ILC precision on aTGCs quoted above already surpasses the precision obtained at LEP on the electroweak observables. A global fit including Higgs, TGC and the Z -pole measurements would be instructive but is beyond the scope of this paper.

3.5 Global fit and determinant parameter

Our total χ^2 can be rewritten as the sum of that of the measurements described previously in this section:

$$\chi_{\text{tot}}^2 = \chi_{hZ/\nu\bar{\nu}h, \text{rates}}^2 + \chi_{hZ, \text{asymmetries}}^2 + \chi_{WW}^2, \quad (3.4)$$

where⁷

$$\chi_{hZ/\nu\bar{\nu}h, \text{rates}}^2 = \sum_i \frac{(\mu_i^{\text{NP}} - \mu_i^{\text{SM}})^2}{\sigma_{\mu_i}^2}, \quad (3.5)$$

$$\chi_{hZ, \text{asymmetries}}^2 = \sum_i \frac{(\mathcal{A}_i^{\text{NP}} - \mathcal{A}_i^{\text{SM}})^2}{\sigma_{\mathcal{A}_i}^2}, \quad (3.6)$$

$$\chi_{WW(\text{CEPC \& FCC-ee})}^2 = \sum_i \frac{(n_i^{\text{NP}} - n_i^{\text{SM}})^2}{(\sqrt{n_i} + \sigma_i^{\text{sys}})^2}. \quad (3.7)$$

The μ_i are the signal strengths (rates normalized to SM predictions) of the rate measurements, summed over $\sigma(hZ)$, $\sigma(hZ) \times \text{BR}$ and $\sigma(\nu\bar{\nu}h) \times \text{BR}$. The corresponding one-sigma uncertainties are listed in Table 2, 3 and 4 of Appendix B, for the different colliders. \mathcal{A}_i are the asymmetries of Eq. (3.2), and $\sigma_{\mathcal{A}_i}$ their uncertainties, given in Eq. (3.3). For the $e^+e^- \rightarrow WW$ measurements at CEPC and FCC-ee, the χ^2 is summed over all W -boson decay channels, over the five angular distributions, and over all their bins. A systematic uncertainty σ_i^{sys} is included in each bin. Unless otherwise specified, we take $\sigma_i^{\text{sys}}/n_i = 1\%$ where n_i is the number of events in that bin. For ILC and CLIC, the χ_{WW}^2 is directly

⁶See also Ref. [25] for a recent discussion on this topic in the context of LHC measurements.

⁷Note that we have used the symbol σ to denote both cross sections and standard deviations. What we mean in each case should be clear from the context.

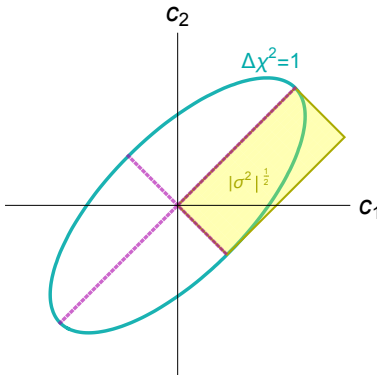


Figure 6: In a two-dimensional parameter space, the area of the Gaussian one-sigma ellipse is proportional to the square root of the determinant of the covariance matrix, $\sqrt{\det \sigma^2}$. In n dimensions, the n th root of this quantity or *global determinant parameter* (GDP $\equiv \sqrt[n]{\det \sigma^2}$) provides an average of constraints strengths. GDP ratios measure improvements in global constraint strengths independently of an effective-field-theory operator basis.

reconstructed from one-sigma bounds and the correlation matrix of aTGCs from Ref. [68] (shown in Table 7 of Appendix B). Finally, the χ^2 is summed over runs with different energies and beam polarizations (if applicable).

As we only retained the linear dependence of all observables in terms of effective-operator coefficients, our χ^2 are quadratic functions:

$$\chi^2 = \sum_{ij} (c - c_0)_i \sigma_{ij}^{-2} (c - c_0)_j, \quad \text{where} \quad \sigma_{ij}^{-2} \equiv (\delta c_i \rho_{ij} \delta c_j)^{-1}, \quad (3.8)$$

where $c_{i=1, \dots, 12}$ denotes the 12 parameters of Eq. (2.1) and c_0 are the corresponding central values, which are vanishing by construction in our study. The uncertainties δc_i and the correlation matrix ρ can thus be obtained from $\sigma_{ij}^{-2} = \partial^2 \chi^2 / \partial c_i \partial c_j$.

It should also be noted that the measured Higgs decay width reported in the corresponding documents of the colliders is a quantity derived (with certain assumptions) from several measurements which are already included in the fit. We therefore do not include it in our fit as an additional independent measurement.

Global determinant parameter (GDP) We introduce a metric, dubbed *global determinant parameter*, for assessing the overall strength of constraints. In a global analysis featuring n degrees of freedom, it is defined as the determinant of the covariance matrix raised to the $1/2n$ power, $\text{GDP} \equiv \sqrt[n]{\det \sigma^2}$. In a multivariate Gaussian problem, the square root of the determinant is proportional to the volume of the one-sigma ellipsoid ($\pi^{\frac{n}{2}} / \Gamma(\frac{n}{2} + 1) \sqrt{\det \sigma^2}$) and therefore measures the allowed parameter space size (see Fig. 6). Its n th root is the geometric average of the half lengths of the ellipsoid axes and can thus serve as an average constraint strength. Interestingly, the ellipsoid volume transforms linearly under rescalings of the fit parameters. So, ratios of GDPs do not depend

on parameters' normalization. They are obviously also invariant under rotations in the multidimensional parameters space. Such ratios are thus independent on the choice of effective-operator basis used to describe the same underlying physics. We therefore judge these quantities especially convenient to measure the improvement in global constraints brought by different run scenarios of future lepton colliders. It is however to be noted that the GDP measure weights equally all directions in the effective-field-theory parameter space, so that it is on its own certainly not accounting for the fact some directions are privileged by specific power countings or models.

4 Results

We first discuss in this section the precision reach of the whole program of each collider before examining, in subsequent subsections, the impact of different measurements, center-of-mass energies, systematic uncertainties, and beam polarization. The CEPC is then taken as an illustrative example (except when studying polarization) and the corresponding figures for the FCC-ee and ILC are provided in [Appendix C](#).

We show in [Fig. 7](#) the one-sigma precision reach at various future lepton colliders on our effective-field-theory parameters. These projections are compared to the reach of the Higgs measurements at the 14 TeV LHC with 300 fb^{-1} and 3000 fb^{-1} of integrated luminosity, combined with the diboson production measurement at LEP. The estimated reach of Higgs measurements at the high-luminosity LHC derives from projection by the ATLAS collaboration [\[73\]](#) which collected information from various other sources. Information about the composition of each channel are extracted from Ref. [\[74–78\]](#). Theory uncertainties on these LHC measurements are not included in our estimations. In LHC results, we also assume the charm Yukawa to be SM-like as Ref. [\[73\]](#) does not provide estimations on the $h \rightarrow c\bar{c}$ branching fraction precision reach. The constraints from the diboson measurements at LEP are obtained from Ref. [\[23\]](#). We do not include the LHC constraints arising from diboson production, as issues related to the validity of the effective-field-theory [\[79, 24\]](#) and of the TGC dominance assumption [\[25\]](#) need to be simultaneously considered. A dedicated study of the reach of the high-luminosity LHC on these processes should be carried out. The constraints set at future lepton colliders are however expected to be much more stringent.

Compared with LHC and LEP, future lepton colliders would improve the measurements of effective-field-theory parameters by roughly one order of magnitude. A combination with the LHC measurements provides a marginal improvement for most of the parameters. For $\bar{c}_{\gamma\gamma}$, $\bar{c}_{Z\gamma}$ and δy_μ , the improvements are more significant, as the small rates and clean signals make the LHC reaches comparable to that of lepton colliders. It should be noted that the measurements of the $h \rightarrow gg$ branching fraction only constrain a linear combination of \bar{c}_{gg} and δy_t . These two parameters are thus only constrained independently by lepton colliders when $t\bar{t}h$ production is measured. Therefore, the combination with LHC measurements is required for CEPC and FCC-ee to constrain \bar{c}_{gg} and

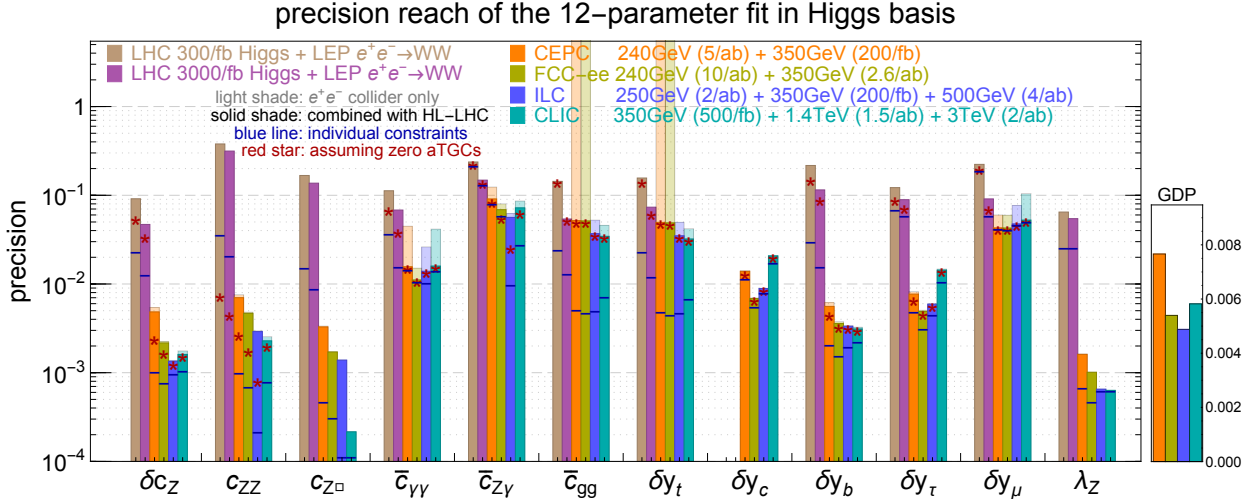


Figure 7: One-sigma precision reach of future lepton colliders on our effective-field-theory parameters. All results but the light-shaded columns include the 14 TeV LHC (with 3000 fb^{-1}) and LEP measurements. LHC constraints also include measurements carried out at 8 TeV. Note that, without run above the $t\bar{t}h$ threshold, circular colliders alone do not constrain the \bar{c}_{gg} and δy_t effective-field-theory parameter individually. The combination with LHC measurements however resolves this flat direction. The horizontal blue lines on each column correspond to the constraints obtained when one single parameter is kept at the time, assuming all others vanish. The red stars correspond to the constraints assuming vanishing aTGCs. The GDPs of future lepton colliders are shown on the right panel. See main text for comparisons with the LHC GDPs.

δy_t . The resulting bounds on δy_t are then even substantially better than that set by the LHC alone.

The twelve-parameter GDPs for the combination of future lepton collider, LHC 3000 fb^{-1} and LEP measurements are displayed on the right panel of Fig. 7. Corresponding numerical values are 0.0077, 0.0054, 0.0049, 0.0058 for CEPC, FCC-ee, ILC and CLIC, respectively. Varying prospective constraints on the charm Yukawa measurement complicate the comparison with the high-luminosity LHC. The ATLAS collaboration estimated the $h \rightarrow J/\psi \gamma$ branching fraction could be constrained to be smaller than 15 times its standard model value with 3 ab^{-1} at 14 TeV [80]. Such a constraint would translate into a one-sigma precision reach on δy_c of order one. To broadly cover the range spent by other studies [81–85], we vary the expected precision reach on δy_c in the $0.01 - 10$ range. The combination of LHC 300 fb^{-1} (3000 fb^{-1}) and LEP measurements only then leads to GDPs in the $0.065 - 0.116$ ($0.039 - 0.069$) interval, one order of magnitude worst than when future lepton collider measurements are included. On the other hand, with δy_c set to zero, the eleven-parameter GDP for the combination of LHC 300 fb^{-1} (3000 fb^{-1}) and LEP measurements only is of 0.078 (0.044). In comparison, when future lepton collider measurements are also included, the corresponding eleven-parameter GDP are 0.0073,

0.0053, 0.0046, 0.0052 for CEPC, FCC-ee, ILC and CLIC, respectively.

Let us also comment further on the impact of having discarded the quadratic dependence on dimension-six operator coefficients. As stressed in [Section 2](#), no significant effect is expected given the good precision achieved at future lepton colliders in the measurement of most observable. Note that even the branching ratios for rare Higgs decays like $h \rightarrow \gamma Z$ are sufficiently well constrained for quadratic contributions to be subleading. Only cases in which accidental suppressions of the standard-model interference with effective-field-theory amplitudes require a case-by-case discussion. We identify two such cases. First, helicity selection rules are known to suppress the ratio of linear and quadratic dependences on the λ_Z aTGC at high energies. Reproducing the analysis made at 250 GeV for a center-of-mass energy of 500 GeV and 500 fb^{-1} shared between two beam polarization configurations, with and without quadratic aTGC contributions, we obtained differences in the derived limits of 10% at most. The linear approximation thus seems to be reasonably accurate in that case and no strong quadratic aTGC dependence should affect the bounds derived in Ref. [\[68\]](#). We also checked that quadratic contributions would be subleading at $\sqrt{s} = 3 \text{ TeV}$, provided the whole differential information is included. The non-interference between standard-model and dimension-six operator indeed does not hold when the azimuthal angles of the W decay products are not integrated over. Secondly, as noted in [Section 3.1](#), the interference between the s -channel photon and Z amplitudes in the unpolarized Higgsstrahlung cross section suffers from an accidental numerical suppression. Moreover, at high energies, the Higgsstrahlung cross section goes down and so does the accuracy with which it can be measured. Therefore, one can expect the quadratic dependence on the operator modifying the $HZ\gamma$ vertex with an off-shell photon to be important in that specific case. Although we use unpolarized cross section measurements to determine CLIC reach on effective-field-theory parameters to match experimental studies, beam polarization would actually be available at CLIC and we checked explicitly that the quadratic effective-field-theory contributions become unimportant once measurements with polarized beams are performed.

4.1 Impact of the various measurements

We examine, in [Fig. 8](#), the impact of different measurements. The one-sigma precision are displayed with one or more measurements removed from the global fit, using CEPC as an example. Since the degeneracy between \bar{c}_{gg} and δy_t can not be resolved with measurements at 240 and 350 GeV, we display the constraint on $\bar{c}_{gg}^{\text{eff}}$, defined in [Eq. \(2.3\)](#). The first five columns use the measurements at 240 GeV (5 ab^{-1}) only. The first column on the left shows the results from rate measurements in Higgs processes ($e^+e^- \rightarrow hZ/\nu\bar{\nu}h$) only. To obtain the second, third, and fourth columns, one single measurement is excluded at the time: $e^+e^- \rightarrow WW$ (2nd), $e^+e^- \rightarrow \nu\bar{\nu}h$ (3rd), and the angular asymmetries of $e^+e^- \rightarrow hZ$ (4th), respectively. The fifth column expresses the constraints deriving from all measurements at 240 GeV. In the last column, 200 fb^{-1} of data at 350 GeV is also included. The dark shades finally display the constraints deriving when one single

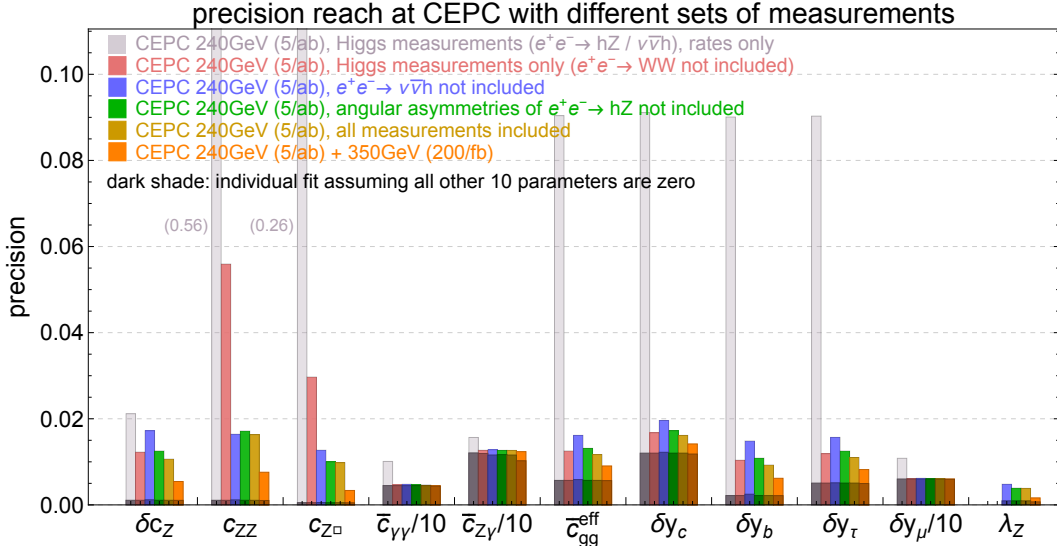


Figure 8: One-sigma precision reach obtained with various combinations of measurements at the CEPC. The first five columns exploit 5 ab^{-1} of 240 GeV data while the last column also includes 200 fb^{-1} at 350 GeV. Only Higgs rate measurements ($e^+e^- \rightarrow hZ/\nu\bar{\nu}h$) are included in the first column. One single measurement is excluded at the time in the three subsequent columns: $e^+e^- \rightarrow WW$ in the second, $e^+e^- \rightarrow \nu\bar{\nu}h$ in the third, and the angular asymmetries of $e^+e^- \rightarrow hZ$ in the fourth. Note that λ_Z is left unconstrained by Higgs data. All measurements at 240 GeV are included to obtain the constraints in the fifth column. A run at 350 GeV is also included in the last, sixth, column. The dark shades correspond to the constraints obtained when one single parameter is kept at the time, assuming all other vanish.

effective-field-theory parameter is kept at a time.

Figure 8 transparently demonstrates that the Higgs rate measurements alone are insufficient to constrain simultaneously all parameters to a satisfactory degree. They leave poorly constrained some directions of the multidimensional parameter space, thereby weakening the whole fit. As already stressed, in such a global treatment, the combination of several observables is capital to effectively bound all parameter combinations. The global strength of constraints is dramatically improved by the first few measurement which resolve approximate degeneracies. Once a sufficient number of constraints is imposed, the exclusion of one single observable does not dramatically affect the overall precision. The individual constraints (obtained by switching on one parameter at a time), on the other hand, receive little improvement from the additional measurements — a clear demonstration that global constraints are driven by approximate degeneracies. A marginal improvement of the constraints obtained for a given run would be obtained by including a set of observables even more complete than the one we use.

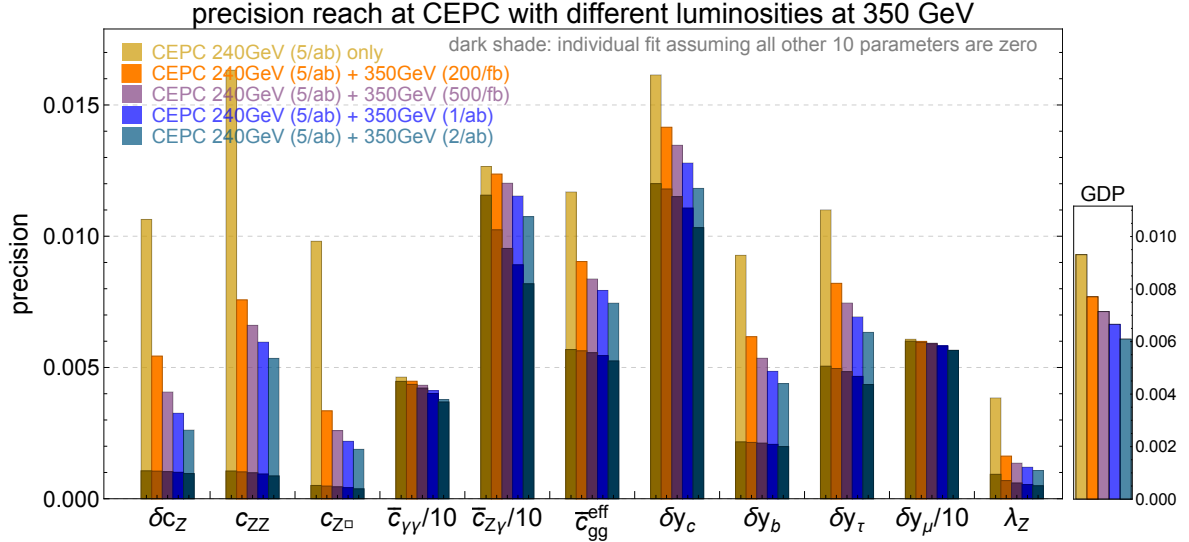


Figure 9: Precision reach (one standard deviation) of the 11-parameter fit in the Higgs basis at CEPC. Five different assumptions on the luminosity at 350 GeV are made, namely 0 (240 GeV run only), 200 fb^{-1} , 500 fb^{-1} , 1 ab^{-1} and 2 ab^{-1} (from left to right). The luminosity at 240 GeV is fixed to 5 ab^{-1} . The parameters $\bar{c}_{\gamma\gamma}$, $\bar{c}_{Z\gamma}$ and $\bar{c}_{gg}^{\text{eff}}$ are defined in Eq. (2.2) and Eq. (2.3). The dark shades correspond to the constraints obtained when one single parameter is kept at the time, assuming all others vanish.

4.2 Impact of a 350 GeV run at circular colliders

As already visible in Fig. 8, a 350 GeV run significantly improves the strength of the constraints set by circular colliders. An important question for their design is the optimal amount of luminosity to gather at that energy, in view of the physics performance and the budget cost. In addition to the top mass and electroweak coupling measurements, the improvement on the precision of Higgs coupling could be considered too. This is addressed in Fig. 9 which shows the reach of the CEPC for increasing amounts of integrated luminosity collected at 350 GeV, from 0 to 2 ab^{-1} . It is clear that a run at this energy is able to lift further approximate degeneracy among effective-field-theory parameters. A GDP reduction of about 17% is obtained with only 200 fb^{-1} , and reaches about 34% with 2 ab^{-1} . The improvements on the $\bar{c}_{\gamma\gamma}$, $\bar{c}_{Z\gamma}$, and δy_μ effective parameters are less significant. The Higgs decay channels which provide the dominant constraints on these parameters suffer from small rates. These constraints are thus mainly statistics limited and approximate degeneracies play a secondary role. It should be noted that the estimations for Higgs measurements at 350 GeV for various luminosities are obtained by scaling from the ones in Table 2, assuming statistical uncertainties dominate. This assumption may cease to be valid for large integrated luminosities.

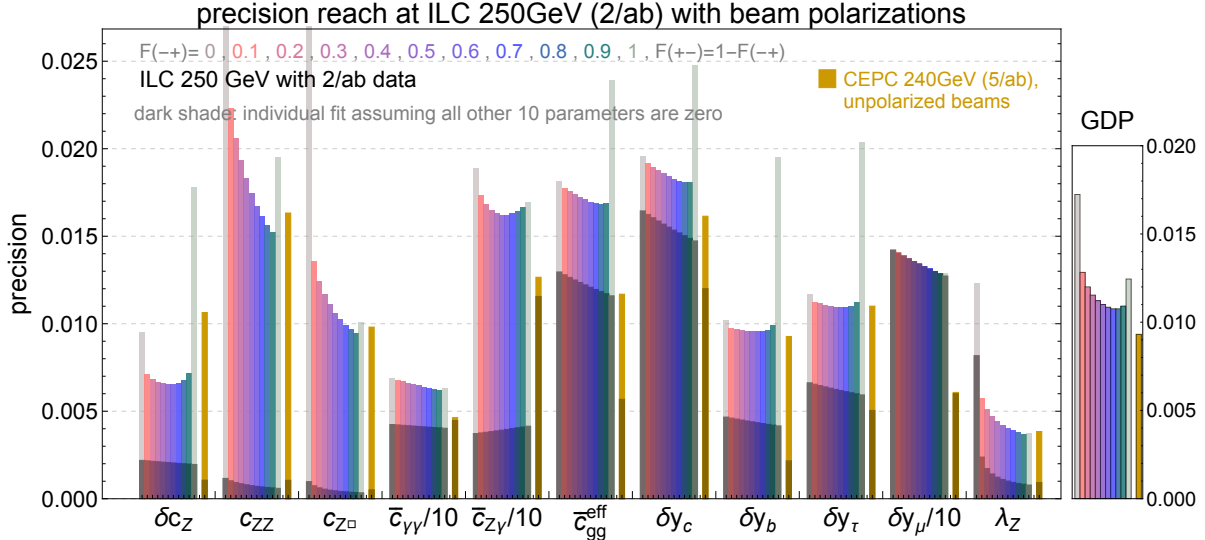


Figure 10: One-sigma precision reach of ILC runs at 250 GeV with 2ab^{-1} of integrated luminosity shared between $P(e^-, e^+) = (-0.8, +0.3)$ and $(+0.8, -0.3)$ beam polarization configurations. The corresponding fractions are denoted as $F_{(-+)}$ and $F_{(+-)} = 1 - F_{(-+)}$. For the sake of comparison, the constraints resulting from a CEPC run at 240 GeV with 5ab^{-1} of integrated luminosity collected without beam polarization are also shown. The dark shades correspond to the constraints obtained when one single parameter is kept at the time, assuming all others vanish.

4.3 Impact of beam polarization at linear colliders

The possibility of longitudinal beam polarization constitutes a distinct advantage for linear colliders. Implementing it at circular colliders may be difficult (especially at high center-of-mass energies) and not economically feasible [2]. Dividing the total luminosity into multiple runs of different polarization configurations effectively provides several independent observables and helps constraining different direction of the effective-theory parameter space. In Fig. 10, we examine what subdivision of the total ILC luminosity at 250 GeV would optimize the final precision reach. We follow the ILC TDR [3] and assume that the ILC could achieve a maximum beam polarization of 80% for electrons and 30% for positrons. Ref. [58] proposes a run plan with four polarization configurations $\text{sgn}\{P(e^-, e^+)\} = (-, +), (+, -), (-, -), (+, +)$ and corresponding luminosity fractions of 67.5%, 22.5%, 5%, and 5%, respectively. The $(-, -)$ and $(+, +)$ polarizations could serve to probe exotic new physics, like electron dipole or Yukawa operators. They however suppress the rate of Higgs and gauge boson production and are thus not very helpful for the precision study of these processes. For simplicity, we will thus only consider the $(-, +)$ and $(+, -)$ polarizations. Uncertainty estimates are often only provided for an entire run in the $P(e^-, e^+) = (-0.8, +0.3)$ configuration. Scaling with statistics is performed to obtain estimates for other scenarios, assuming no correlation among the measurements carried out with different polarizations. In agreement with the proposal of Ref. [58],

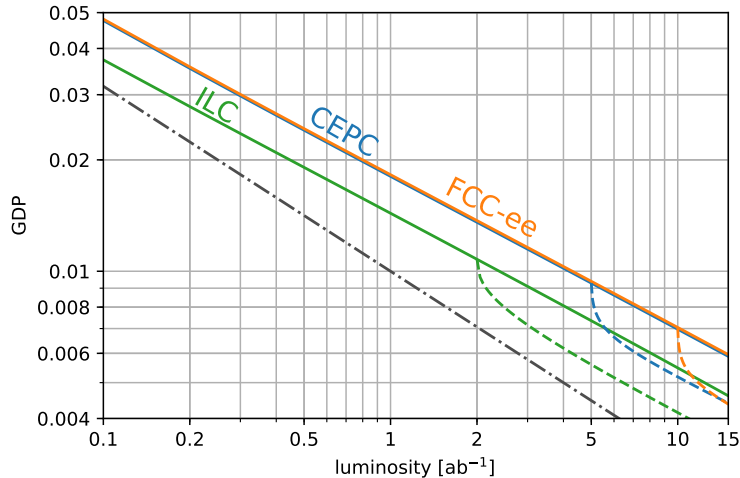


Figure 11: Global GDP strength of the constraints in our eleven-dimensional parameter space as a function the luminosity collected, without beam polarization, at a center-of-mass energy of 240 GeV (for the CEPC and FCC-ee) and at 250 GeV, with polarized beams (for the ILC). The dashed lines show the improvements brought by subsequent runs at 350 GeV. A pure statistical scaling of constraints, in the absence of systematic uncertainties, would have led to the slope of the dot-dashed line.

Fig. 10 shows that the best overall constraints are obtained with about 70% of the 2 ab^{-1} ILC luminosity at 250 GeV spent with $P(e^-, e^+) = (-0.8, +0.3)$ beam polarization and 30% with $P(e^-, e^+) = (+0.8, -0.3)$. The $(-0.8, +0.3)$ polarization enhances the cross section, while the $(+0.8, -0.3)$ one helps resolving degeneracies. In terms of GDP, this optimal repartition of luminosity provides results that are 14% better than a full run with $P(e^-, e^+) = (-0.8, +0.3)$ beam polarization. For comparison, we also show the reach of a 240 GeV CEPC run with 5 ab^{-1} of integrated luminosity and unpolarized beams. The higher luminosity is able compensate for the lack of polarization and comparable overall results are obtained. This is further quantified by Fig. 11 which displays the GDP of our eleven-parameter fit as a function of luminosity collected at 250 GeV with polarized beams and at 240 GeV with unpolarized ones. It is notably seen that only about 1.5 ab^{-1} of additional luminosity are required without polarized beams to match the overall performance obtained with 2 ab^{-1} of polarized beams. With 5 ab^{-1} and 10 ab^{-1} collected at 240 GeV, the CEPC and FCC-ee reach GDPs respectively 14% and 34% smaller than that of the full ILC run (2 ab^{-1}) at 250 GeV.

4.4 Impact of systematic uncertainties in diboson production

Another important issue concerns the impact of systematic uncertainties on the constraints deriving from $e^+e^- \rightarrow WW$ measurements. As discussed earlier, they have not yet

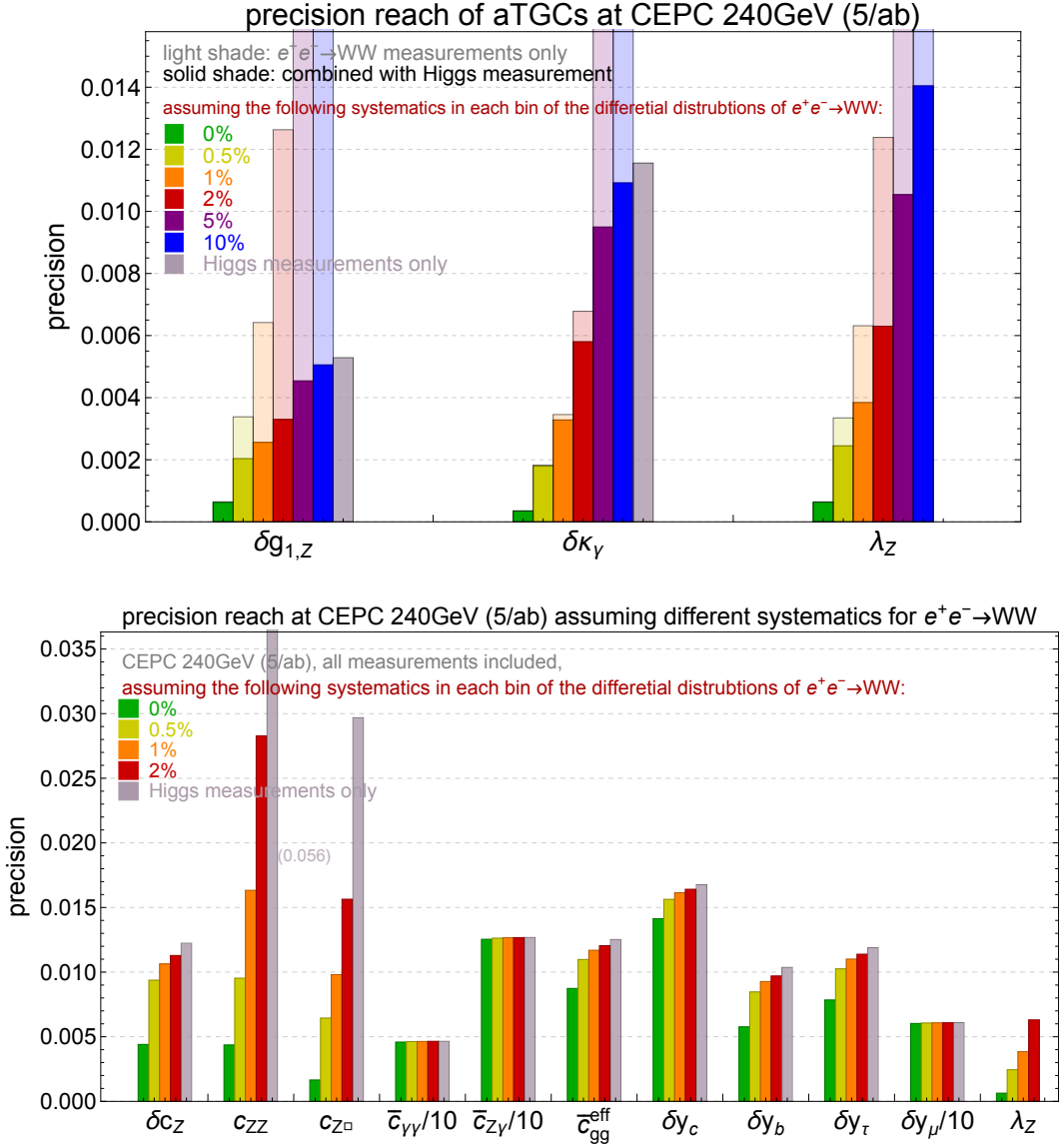


Figure 12: *Top*: One-sigma constraints on aTGCs parameters for different assumptions about the systematic uncertainties affecting the $e^+e^- \rightarrow WW$ measurements at the CEPC. Each of the five angular distributions is divided into 20 bins (or 10 bins for the angles characterizing W decays in indistinguishable quark-antiquark pairs). We assume a fixed relative uncertainty each bin, and no correlation among them. A benchmark value of 1% is used elsewhere in this paper, for CEPC and FCC-ee measurements. *Bottom*: One-sigma reach of the 240 GeV CEPC run for different systematic uncertainties in the differential measurements of diboson production.

been determined by dedicated experimental studies except for the 500 GeV ILC run. The top panel of Fig. 12 focuses on the aTGC parameters $\delta g_{1,Z}$, $\delta\kappa_\gamma$, and λ_Z . Systematic uncertainties ranging between 0 and 10% are assumed in each bin of the $e^+e^- \rightarrow WW \rightarrow 4f$ angular distributions. The constraints derived from diboson production only are shown in lighter shades. Darker shades show their combination with Higgs measurements, which alone give the gray limits (leaving λ_Z unconstrained). It is noted that the Higgs measurement constraints on these TGC parameters are improved as soon as uncertainties fall below 10%. On the other hand, Higgs measurements still bring improvements to aTGCs determination when systematic uncertainties fall to 0.5%. The improvement on the whole fit brought by the combination of Higgs and $e^+e^- \rightarrow WW \rightarrow 4f$ measurements of varying systematic uncertainties is displayed in Fig. 12. As shown in Eq. (A.6), two of the TGC parameters, $\delta g_{1,Z}$, and $\delta\kappa_\gamma$, are related to c_{ZZ} , $c_{Z\Box}$, $c_{\gamma\gamma}$, $c_{Z\gamma}$ in Higgs measurements. The constraints on the c_{ZZ} , $c_{Z\Box}$, and λ_Z effective-field-theory parameters are benefiting the most from a reduction of systematic uncertainties in diboson production measurements. Improvements are limited for $c_{\gamma\gamma}$ and $c_{Z\gamma}$ which are already well constrained by the measurements of the $h \rightarrow \gamma\gamma$ and $h \rightarrow Z\gamma$ decays.

As our conservative estimate of systematic uncertainties often render the $e^+e^- \rightarrow WW$ measurements systematics dominated, we show for comparison the results that would have been obtained with perfect TGC constraints with red stars on Fig. 7. The Fig. 13 in Appendix C also contains more detailed fit results under this assumption.

4.5 Comparison with previous global analyses

Comparing our results with the ones in Refs. [32, 35], a few important differences should be noted. Different assumptions have been made for the run plans of some colliders. In particular, we adopted the most recent ILC run scenario for ILC described in Refs. [57, 58], while Ref. [32] assumed only 250 fb^{-1} would be collected at 250 GeV. Contrarily to Refs. [32, 35], we also lift the flavor-universality assumption on Yukawa modifications. Information about the $e^+e^- \rightarrow hZ$ angular distributions were not included in these existing global analyses. Our respective treatments for the TGC measurements, for which no dedicated experimental study has been carried out, is also different. Reference [35] also addressed the potential of CLIC in probing the Higgsstrahlung process and measuring TGCs at 1.4 and 3 TeV. Their estimations for the measurements of $\sigma(hZ) \times \text{BR}(h \rightarrow b\bar{b})$ at 1.4 and 3 TeV are adopted in our study.

5 Conclusions

Future lepton colliders running at center-of-mass energies of around 240 GeV and above are ideal to narrow down the Higgs boson properties, examine the fine details of the electroweak symmetry breaking mechanism and indirectly reveal new physics. Applicable in a low-energy limit, the standard-model effective field theory provides a consistent

model-independent framework to parametrize systematically the theory space in direct vicinity of the standard model. We performed, in this paper, a global effective-field-theory analysis of measurements planned at the CEPC, ILC, FCC-ee and CLIC. A basis-independent metric, GDP ratios, was introduced to assess the global strengthening of constraints obtained in different scenarios. We stressed that a consistent effective-field-theory treatment should be global and that the combination of various measurements is crucial to constrain effectively all directions of its multidimensional parameter space. We considered the $e^+e^- \rightarrow hZ$ rates in its various channels as well as angular distributions, the measurement of Higgs production through weak-boson fusion, and that of weak-boson pair production sensitive to anomalous triple gauge couplings which are related to Higgs interactions. Under assumptions discussed in detail, a twelve-dimensional parameter space describes effective-field-theory contributions to the above observables. We demonstrated that measurements carried out at different center-of-mass energies, or with different beam polarizations, are very effective in resolving approximate degeneracies among effective-field-theory parameters. While circular colliders could collect more luminosity, their linear analogues can reach higher center-of-mass energies and implement longitudinal beam polarizations. High luminosities collected at hadron collider where production rates are often much larger also help constraining rare but clean processes. In that matter, future circular lepton colliders are likely to give way to the next generation of proton colliders reaching 100 TeV center-of-mass energies (the SppC after CEPC [1] and FCC-hh after FCC-ee [56]).

Several improvements to the present analysis are possible. Considering a more complete set of differential observables could obviously strengthen slightly the overall constraints. Quantities that suffer from reduced statistical or systematical uncertainties could also be studied. An important issue which remains to be examined in details concerns the loop-level handles available to constrain the top Yukawa operator below the $t\bar{t}h$ threshold, and around Higgsstrahlung cross section peak in particular. What impact our limited knowledge of electroweak precision observables would have in a global analysis is also a question that should be addressed. Runs at the Z pole or WW threshold may indeed be required to take full advantage of the higher-energy ones. Finally, experimental studies of the weak-boson pair production would be highly valuable to make realistic estimates of the physics potential of future lepton colliders in probing electroweak symmetry breaking.

Acknowledgments

We thank Adam Falkowski, Zhen Liu, Marc Montull, Michael Peskin, Manqi Ruan, Wei Su, Lian-Tao Wang and Xiangpeng Wang for useful discussions, and James Brau, John Ellis, Jenny List, Zhen Liu, Philipp Roloff, Veronica Sanz and Tevong You for valuable comments on the manuscript. We thank Jürgen Reuter and Jenny List for pointing out the importance of the ILC runs at higher energy, Michelangelo Mangano for suggestions on the normalization of the plots, and Thibaud Vantalon for providing us with quadratic EFT dependences. CG is supported by the European Commission through the Marie

Curie Career Integration Grant 631962 and by the Helmholtz Association through the recruitment initiative. JG and KW are supported by an International Postdoctoral Exchange Fellowship Program between the Office of the National Administrative Committee of Postdoctoral Researchers of China (ONACPR) and DESY. We also thank the Collaborative Research Center SFB676 of the Deutsche Forschungsgemeinschaft (DFG), Particles, Strings and the Early Universe, for support.

A Effective-field-theory parameter definitions

We define here our effective-field-theory parameters which are closely related to that of the Higgs basis [39]. As explained in Section 2, our framework is based on that of Ref. [16, 23] where electroweak precision observables are assumed to be standard-model like, and where fermion dipole as well as CP-odd operators are discarded. The assumption of flavor universality for Yukawa operators is however relaxed and we include possible modifications of that of the top, charm, bottom, tau, and muon. The expression of our twelve effective-field-theory parameters in the SILH' basis of dimension-six operators is provided at the end of this section.

The relevant terms in the potential are

$$\mathcal{L} \supset \mathcal{L}_{hVV} + \mathcal{L}_{hff} + \mathcal{L}_{tgc}, \quad (\text{A.1})$$

where the coupling of Higgs boson to a pair of SM gauge bosons are given by

$$\begin{aligned} \mathcal{L}_{hVV} = \frac{h}{v} & \left[(1 + \delta c_W) \frac{g^2 v^2}{2} W_\mu^+ W_\mu^- + (1 + \delta c_Z) \frac{(g^2 + g'^2) v^2}{4} Z_\mu Z_\mu \right. \\ & + c_{WW} \frac{g^2}{2} W_{\mu\nu}^+ W_{\mu\nu}^- + c_{W\Box} g^2 (W_\mu^- \partial_\nu W_{\mu\nu}^+ + \text{h.c.}) \\ & + c_{gg} \frac{g_s^2}{4} G_{\mu\nu}^a G_{\mu\nu}^a + c_{\gamma\gamma} \frac{e^2}{4} A_{\mu\nu} A_{\mu\nu} + c_{Z\gamma} \frac{e\sqrt{g^2 + g'^2}}{2} Z_{\mu\nu} A_{\mu\nu} \\ & \left. + c_{ZZ} \frac{g^2 + g'^2}{4} Z_{\mu\nu} Z_{\mu\nu} + c_{Z\Box} g^2 Z_\mu \partial_\nu Z_{\mu\nu} + c_{\gamma\Box} g g' Z_\mu \partial_\nu A_{\mu\nu} \right]. \quad (\text{A.2}) \end{aligned}$$

Not all the couplings in Eq. (A.2) are independent. In particular, imposing gauge invariance, we rewrite the following couplings as

$$\begin{aligned} \delta c_W &= \delta c_Z + 4\delta m, \\ c_{WW} &= c_{ZZ} + 2s_{\theta_W}^2 c_{Z\gamma} + s_{\theta_W}^4 c_{\gamma\gamma}, \\ c_{W\Box} &= \frac{1}{g^2 - g'^2} \left[g^2 c_{Z\Box} + g'^2 c_{ZZ} - e^2 s_{\theta_W}^2 c_{\gamma\gamma} - (g^2 - g'^2) s_{\theta_W}^2 c_{Z\gamma} \right], \\ c_{\gamma\Box} &= \frac{1}{g^2 - g'^2} \left[2g^2 c_{Z\Box} + (g^2 + g'^2) c_{ZZ} - e^2 c_{\gamma\gamma} - (g^2 - g'^2) c_{Z\gamma} \right], \quad (\text{A.3}) \end{aligned}$$

where δm parameterizes custodial symmetry breaking effects which are set to zero in our framework. While the modifications of Yukawa couplings are, in general, 3×3 complex matrices in generation space, we only consider the diagonal elements relevant for the measurements considered, which are

$$\mathcal{L}_{hff} = -\frac{h}{v} \sum_{f=t,c,b,\tau,\mu} m_f (1 + \delta y_f) \bar{f}_R f_L + \text{h.c.} \quad (\text{A.4})$$

Finally, the triple gauge couplings are given by

$$\begin{aligned} \mathcal{L}_{\text{tgc}} = & \quad ig s_{\theta_W} A^\mu (W^{-\nu} W_{\mu\nu}^+ - W^{+\nu} W_{\mu\nu}^-) \\ & + ig (1 + \delta g_1^Z) c_{\theta_W} Z^\mu (W^{-\nu} W_{\mu\nu}^+ - W^{+\nu} W_{\mu\nu}^-) \\ & + ig [(1 + \delta \kappa_Z) c_{\theta_W} Z^{\mu\nu} + (1 + \delta \kappa_\gamma) s_{\theta_W} A^{\mu\nu}] W_\mu^- W_\nu^+ \\ & + \frac{ig}{m_W^2} (\lambda_Z c_{\theta_W} Z^{\mu\nu} + \lambda_\gamma s_{\theta_W} A^{\mu\nu}) W_\nu^- W_{\rho\mu}^+, \end{aligned} \quad (\text{A.5})$$

where $V_{\mu\nu} \equiv \partial_\mu V_\nu - \partial_\nu V_\mu$ for $V = W^\pm, Z, A$. Imposing gauge invariance, one obtains $\delta \kappa_Z = \delta g_{1,Z} - t_{\theta_W}^2 \delta \kappa_\gamma$ and $\lambda_Z = \lambda_\gamma$, and the contribution from NP can be parameterized by 3 aTGCs, $\delta g_{1,Z}$, $\delta \kappa_\gamma$ and λ_Z . $\delta g_{1,Z}$ and $\delta \kappa_\gamma$ are related to the Higgs observables and can be expressed as

$$\begin{aligned} \delta g_{1,Z} &= \frac{1}{2(g^2 - g'^2)} \left[-g^2(g^2 + g'^2) c_{Z\Box} - g'^2(g^2 + g'^2) c_{ZZ} + e^2 g'^2 c_{\gamma\gamma} + g'^2(g^2 - g'^2) c_{Z\gamma} \right], \\ \delta \kappa_\gamma &= -\frac{g^2}{2} \left(c_{\gamma\gamma} \frac{e^2}{g^2 + g'^2} + c_{Z\gamma} \frac{g^2 - g'^2}{g^2 + g'^2} - c_{ZZ} \right). \end{aligned} \quad (\text{A.6})$$

To summarize, under the assumptions we make, the contribution from dimension-six operators to the potential in Eq. (A.1) can be parameterized by the following non-redundant set of 12 parameters:

$$\delta c_Z, \quad c_{ZZ}, \quad c_{Z\Box}, \quad c_{\gamma\gamma}, \quad c_{Z\gamma}, \quad c_{gg}, \quad \delta y_t, \quad \delta y_c, \quad \delta y_b, \quad \delta y_\tau, \quad \delta y_\mu, \quad \lambda_Z. \quad (\text{A.7})$$

It is straightforward to translate results obtained in the Higgs basis to other bases of dimension-six operators. While all non-redundant basis are equivalent, we found the one listed in Table 1 particularly convenient under our assumption that the Z -pole and W -mass measurements are perfectly standard-model like. In this basis, the 12 parameters of Eq. (A.7) are replaced by the following ones,

$$\begin{aligned} \mathcal{L}_{\text{D6}} = & \frac{c_H}{v^2} \mathcal{O}_H + \frac{\kappa_{WW}}{m_W^2} \mathcal{O}_{WW} + \frac{\kappa_{BB}}{m_W^2} \mathcal{O}_{BB} + \frac{\kappa_{HW}}{m_W^2} \mathcal{O}_{HW} + \frac{\kappa_{HB}}{m_W^2} \mathcal{O}_{HB} \\ & + \frac{\kappa_{GG}}{m_W^2} \mathcal{O}_{GG} + \frac{\kappa_{3W}}{m_W^2} \mathcal{O}_{3W} + \sum_{f=t,c,b,\tau,\mu} \frac{c_{y_f}}{v^2} \mathcal{O}_{y_f}, \end{aligned} \quad (\text{A.8})$$

where the normalization of the parameters are also defined. To go from the SILH' basis [13, 14] to the one in Table 1, one simply trades $\mathcal{O}_W, \mathcal{O}_B \rightarrow \mathcal{O}_{WW}, \mathcal{O}_{WB}$ using

$$\mathcal{O}_B = \mathcal{O}_{HB} + \frac{1}{4} \mathcal{O}_{BB} + \frac{1}{4} \mathcal{O}_{WB},$$

$\mathcal{O}_H = \frac{1}{2}(\partial_\mu H^2)^2$	$\mathcal{O}_{GG} = g_s^2 H ^2 G_{\mu\nu}^A G^{A,\mu\nu}$
$\mathcal{O}_{WW} = g^2 H ^2 W_{\mu\nu}^a W^{a,\mu\nu}$	$\mathcal{O}_{y_u} = y_u H ^2 \bar{Q}_L \tilde{H} u_R$
$\mathcal{O}_{BB} = g'^2 H ^2 B_{\mu\nu} B^{\mu\nu}$	$\mathcal{O}_{y_d} = y_d H ^2 \bar{Q}_L H d_R$
$\mathcal{O}_{HW} = ig(D^\mu H)^\dagger \sigma^a (D^\nu H) W_{\mu\nu}^a$	$\mathcal{O}_{y_e} = y_e H ^2 \bar{L}_L H e_R$
$\mathcal{O}_{HB} = ig'(D^\mu H)^\dagger (D^\nu H) B_{\mu\nu}$	$\mathcal{O}_{3W} = \frac{1}{3!} g \epsilon_{abc} W_\mu^{a\nu} W_\nu^b W^{c\rho\mu}$

Table 1: A complete set of CP-even dimension-six operators that contribute to the Higgs and TGC measurements, assuming there is no correction to the Z -pole and W mass measurements and no dipole interaction. We only consider the flavor-conserving component of \mathcal{O}_{y_u} , \mathcal{O}_{y_d} and \mathcal{O}_{y_e} contributing to the top, charm, bottom, tau, and muon Yukawa couplings.

$$\mathcal{O}_W = \mathcal{O}_{HW} + \frac{1}{4}\mathcal{O}_{WW} + \frac{1}{4}\mathcal{O}_{WB}, \quad (\text{A.9})$$

where \mathcal{O}_{WB} is directly related to the Z -pole measurements (S -parameter) and is thus eliminated. The basis in Table 1 is also used in Ref. [17] with a different notation. In particular, the \mathcal{O}_{HW} and \mathcal{O}_{HB} in Table 1 are denoted as \mathcal{O}_W and \mathcal{O}_B in those references, which are different from the \mathcal{O}_W and \mathcal{O}_B in the SILH convention.

The aTGCs in this basis are given by

$$\begin{aligned} \delta g_{1,Z} &= -\frac{\kappa_{HW}}{c_{\theta_w}^2}, \\ \delta \kappa_\gamma &= -\kappa_{HW} - \kappa_{HB}, \\ \lambda_Z &= -\kappa_{3W}, \end{aligned} \quad (\text{A.10})$$

which are obtained from the general results in Ref. [21]. Finally, the expression of our effective-field-theory parameters in terms of the operators in Table 1 are:

$$\begin{aligned} \delta c_Z &= -\frac{1}{2} c_H, \\ c_{ZZ} &= \frac{4}{g^2 + g'^2} (-\kappa_{HW} - t_{\theta_w}^2 \kappa_{HB} + 4c_{\theta_w}^2 \kappa_{WW} + 4t_{\theta_w}^2 s_{\theta_w}^2 \kappa_{BB}), \\ c_{Z\Box} &= \frac{2}{g^2} (\kappa_{HW} + t_{\theta_w}^2 \kappa_{HB}), \\ c_{\gamma\gamma} &= \frac{16}{g^2} (\kappa_{WW} + \kappa_{BB}), \\ c_{Z\gamma} &= \frac{2}{g^2} (\kappa_{HB} - \kappa_{HW} + 8c_{\theta_w}^2 \kappa_{WW} - 8s_{\theta_w}^2 \kappa_{BB}), \\ c_{gg} &= \frac{16}{g^2} \kappa_{GG}, \\ \delta y_f &= -\frac{1}{2} c_H - c_{y_f}. \end{aligned} \quad (\text{A.11})$$

It should be noted that Eq. (A.11) is only valid under the assumptions made in this paper. More general basis translations from the Higgs basis to the SILH' basis (and others) are provided in Ref. [39].

B Measurement inputs

We provide here additional details about the input measurements used in our study, including the Higgs production rates ($e^+e^- \rightarrow hZ$ and $e^+e^- \rightarrow \nu\bar{\nu}h$), the angular asymmetries in $e^+e^- \rightarrow hZ$ and TGC measurements from $e^+e^- \rightarrow WW$. The estimated one-sigma precisions of the Higgs rate measurements are respectively displayed in Table 2 for the CEPC and FCC-ee, in Table 3 for ILC and, in Table 4 for CLIC. When provided, they are respectively extracted from Ref. [86] for the CEPC (which updates the preCDR [1]), Ref. [2] for the FCC-ee, Ref. [58] for the ILC and Ref. [60] for CLIC. For CLIC, we also include the estimations for $\sigma(hZ) \times \text{BR}(h \rightarrow b\bar{b})$ at 1.4 and 3 TeV from Ref. [35]. While these measurements suffer from smaller cross sections, they nevertheless significantly improve the constraints on c_{ZZ} and $c_{Z\Box}$ due to the huge sensitivities at high energies.⁸ We also found the ZZ fusion measurements at CLIC (with $\sigma(e^+e^-h) \times \text{BR}(h \rightarrow b\bar{b})$ measured to a precision of 1.8% (2.3%) at 1.4 TeV (3 TeV) [60]) to have a negligible impact in our analysis.⁹ The numbers highlighted in green are obtained by scaling with luminosity when dedicated estimates are not available. For the ILC, the estimations of signal strengths are summarized in Ref. [58] (Table 13) but only for benchmark run scenarios with smaller luminosities. These are scaled up to the current run plan. For the 350 GeV run of CEPC and FCC-ee, relative precision are rescaled from the 350 GeV ILC ones.¹⁰ The precision of $\sigma(hZ) \times \text{BR}(h \rightarrow Z\gamma)$ is not provided for the FCC-ee and ILC. We thus scale it from the CEPC estimation. While a statistical precision of 2.2% is reported in Ref. [2] for the $\sigma(\nu\bar{\nu}h) \times \text{BR}(h \rightarrow b\bar{b})$ measurement at FCC-ee 240 GeV, it is not clear what assumptions on the $e^+e^- \rightarrow hZ, Z \rightarrow \nu\bar{\nu}$ process are made in obtaining this estimation. Therefore, we scale it with luminosity from the CEPC one. The difference between unpolarized and polarized cross sections are taken into account in these rescalings. Given the moderate statistics in most of the relevant channels, it is reasonable to assume their precision is statistics limited. Nevertheless, it is important for these estimations to be updated by experimental groups in the future.

The constraints from angular observables in $e^+e^- \rightarrow hZ$ are obtained with the method described in Section 3.1, making use of the channels $e^+e^- \rightarrow hZ, Z \rightarrow \ell^+\ell^-, h \rightarrow b\bar{b}, c\bar{c}, gg$. They are included for all the e^+e^- colliders at all energies except for the 1.4 TeV

⁸We thank Tevong You for pointing this out.

⁹It is nevertheless possible to further optimize the precision reach of the cross section measurements of ZZ fusion using judicious kinematic cuts, as pointed out in Ref. [87]. For simplicity, we do not perform such optimizations in our study.

¹⁰A statistical precision of 0.6% is reported in Ref. [2] for the $\sigma(\nu\bar{\nu}h) \times \text{BR}(h \rightarrow b\bar{b})$ measurement at FCC-ee 350 GeV, which is in good agreement with our estimation from scaling (0.71%).

	CEPC				FCC-ee			
	[240 GeV, 5 ab ⁻¹]		[350 GeV, 200 fb ⁻¹]		[240 GeV, 10 ab ⁻¹]		[350 GeV, 2.6 ab ⁻¹]	
	Zh	$\nu\bar{\nu}h$	Zh	$\nu\bar{\nu}h$	Zh	$\nu\bar{\nu}h$	Zh	$\nu\bar{\nu}h$
production								
σ	0.50%	-	2.4%	-	0.40%	-	0.67%	-
	$\sigma \times \text{BR}$				$\sigma \times \text{BR}$			
$h \rightarrow b\bar{b}$	0.21% [★]	0.39% [◇]	2.0%	2.6%	0.20%	0.28% [◇]	0.54%	0.71%
$h \rightarrow c\bar{c}$	2.5%	-	15%	26%	1.2%	-	4.1%	7.1%
$h \rightarrow g\bar{g}$	1.2%	-	11%	17%	1.4%	-	3.1%	4.7%
$h \rightarrow \tau\tau$	1.0%	-	5.3%	37%	0.7%	-	1.5%	10%
$h \rightarrow WW^*$	1.0%	-	10%	9.8%	0.9%	-	2.8%	2.7%
$h \rightarrow ZZ^*$	4.3%	-	33%	33%	3.1%	-	9.2%	9.3%
$h \rightarrow \gamma\gamma$	9.0%	-	51%	77%	3.0%	-	14%	21%
$h \rightarrow \mu\mu$	12%	-	115%	275%	13%	-	32%	76%
$h \rightarrow Z\gamma$	25%	-	144%	-	18%	-	40%	-

Table 2: The estimated precision of CEPC and FCC-ee Higgs measurements. We gather the available estimations from Refs. [1, 2, 86], while the missing ones (highlighted in green) are obtained from scaling with luminosity. See Appendix B for more details. For $\sigma(e^+e^- \rightarrow \nu\bar{\nu}h)$, the precisions marked with a diamond \diamond are normalized to the cross section of the inclusive channel which includes both the WW fusion and $e^+e^- \rightarrow hZ, Z \rightarrow \nu\bar{\nu}$, while the unmarked precisions are normalized to the WW fusion process only. For the CEPC, the precision of the $\sigma(hZ) \times \text{BR}(h \rightarrow b\bar{b})$ measurement (marked by a star \star) reduces to 0.24% if one excludes the contribution from $e^+e^- \rightarrow hZ, Z \rightarrow \nu\bar{\nu}, h \rightarrow b\bar{b}$ to avoid double counting with $e^+e^- \rightarrow \nu\bar{\nu}h, h \rightarrow b\bar{b}$. The corresponding information is not available for the FCC-ee.

and 3 TeV runs of CLIC.

The constraints on aTGCs derived from the $e^+e^- \rightarrow WW$ measurements are obtained using the method described in Section 3.4, for the CEPC and FCC-ee. In particular, 1% systematic uncertainties are assumed in each bin with the differential distribution of each measured angle divided in 20 bins (10 bins if the angle is *folded*). The results, including the correlation matrices, are shown in Table 5 and Table 6, which are fed into the global fit. For ILC, the constraints are shown in Table 7, taken from Ref. [68], which assumes 500 fb⁻¹ data at 500 GeV and four $P(e^-, e^+) = (\pm 0.8, \pm 0.3)$ beam polarization configurations. For CLIC, we simply use the ILC results.

While the measurement inputs of LHC and LEP measurements are too lengthy to be reported in this paper, here we simply list the results from the global fits in terms of one sigma constraints and the correlation matrix, which can be used to reconstruct the chi-square. The chi-square can then be combined with the ones of the future e^+e^- colliders to reproduce the results in Fig. 7 and Table 11. In Table 8, we list the current constraints in Ref. [23], obtained from the LHC 8 TeV Higgs measurements and LEP $e^+e^- \rightarrow WW$ measurements. While Ref. [23] explicitly assumes flavor universality for the Yukawa couplings, it is a good approximation to simply assume the constraints given there apply to third-generation couplings. Since we explicitly assume the future results are SM-like, for consistency, we also set the central values of current results to zero when

ILC

	[250 GeV, 2 ab ⁻¹]		[350 GeV, 200 fb ⁻¹]		[500 GeV, 4 ab ⁻¹]			[1 TeV, 1 ab ⁻¹]		[1 TeV, 2.5 ab ⁻¹]	
production	Zh	$\nu\bar{\nu}h$	Zh	$\nu\bar{\nu}h$	Zh	$\nu\bar{\nu}h$	tth	$\nu\bar{\nu}h$	tth	$\nu\bar{\nu}h$	tth
σ	0.71%	-	2.1%	-	1.1%	-	-	-	-	-	-
	$\sigma \times \text{BR}$										
$h \rightarrow b\bar{b}$	0.42%	3.7%	1.7%	1.7%	0.64%	0.25%	9.9%	0.5%	6.0%	0.3%	3.8%
$h \rightarrow c\bar{c}$	2.9%	-	13%	17%	4.6%	2.2%	-	3.1%	-	2.0%	-
$h \rightarrow gg$	2.5%	-	9.4%	11%	3.9%	1.4%	-	2.3%	-	1.4%	-
$h \rightarrow \tau\tau$	1.1%	-	4.5%	24%	1.9%	3.2%	-	1.6%	-	1.0%	-
$h \rightarrow WW^*$	2.3%	-	8.7%	6.4%	3.3%	0.85%	-	3.1%	-	2.0%	-
$h \rightarrow ZZ^*$	6.7%	-	28%	22%	8.8%	2.9%	-	4.1%	-	2.6%	-
$h \rightarrow \gamma\gamma$	12%	-	44%	50%	12%	6.7%	-	8.5%	-	5.4%	-
$h \rightarrow \mu\mu$	25%	-	98%	180%	31%	25%	-	31%	-	20%	-
$h \rightarrow Z\gamma$	34%	-	145%	-	49%	-	-	-	-	-	-

Table 3: The estimated precision of ILC Higgs measurements. For the 250 GeV, 350 GeV and 500 GeV runs, all numbers are scaled from Ref. [58] (Table 13), except for $\sigma(hZ) \times \text{BR}(h \rightarrow Z\gamma)$ which is scaled from the CEPC estimation. A beam polarization of $P(e^-, e^+) = (-0.8, +0.3)$ is assumed. The 1 TeV run is only included in Fig. 17 of Appendix C, while the estimations are taken from Ref. [59] which assumes a polarization of $P(e^-, e^+) = (-0.8, +0.2)$.

CLIC

	[350 GeV, 500 fb ⁻¹]		[1.4 TeV, 1.5 ab ⁻¹]		[3 TeV, 2 ab ⁻¹]
production	Zh	$\nu\bar{\nu}h$	$\nu\bar{\nu}h$	tth	$\nu\bar{\nu}h$
σ	1.6%	-	-	-	-
	$\sigma \times \text{BR}$				
$h \rightarrow b\bar{b}$	0.84%	1.9%	0.4%	8.4%	0.3%
$h \rightarrow c\bar{c}$	10.3%	14.3%	6.1%	-	6.9%
$h \rightarrow gg$	4.5%	5.7%	5.0%	-	4.3%
$h \rightarrow \tau\tau$	6.2%	-	4.2%	-	4.4%
$h \rightarrow WW^*$	5.1%	-	1.0%	-	0.7%
$h \rightarrow ZZ^*$	-	-	5.6%	-	3.9%
$h \rightarrow \gamma\gamma$	-	-	15%	-	10%
$h \rightarrow \mu\mu$	-	-	38%	-	25%
$h \rightarrow Z\gamma$	-	-	42%	-	30%

Table 4: The estimated precision of CLIC Higgs measurements taken from Ref. [60], which assumes unpolarized beams and considers only statistical uncertainties. In addition, we also include the estimations for $\sigma(hZ) \times \text{BR}(h \rightarrow b\bar{b})$ at high energies in Ref. [35], which are 3.3% (6.8%) at 1.4 TeV (3 TeV). We find the inclusion of the ZZ fusion ($e^+e^- \rightarrow e^+e^-h$) measurements to have little impact in our analysis.

combining them with the future collider results. In Table 9 and 10, we list the results for the 14 TeV LHC with 300 fb⁻¹ and 3000 fb⁻¹ luminosity, derived from projection by the ATLAS collaboration [73] which collected information from various other sources, while the information about the composition of each channel are extracted from Refs. [74–78].

CEPC								
	240 GeV(5 ab ⁻¹)				240 GeV(5 ab ⁻¹)+350 GeV(200 fb ⁻¹)			
	uncertainty	correlation matrix			uncertainty	correlation matrix		
		$\delta g_{1,Z}$	$\delta\kappa_\gamma$	λ_Z		$\delta g_{1,Z}$	$\delta\kappa_\gamma$	λ_Z
$\delta g_{1,Z}$	0.0064	1	0.068	-0.93	0.0037	1	-0.51	-0.89
$\delta\kappa_\gamma$	0.0035		1	-0.40	0.0017		1	0.12
λ_Z	0.0063			1	0.0030			1

Table 5: The constraints on aTGCs from the $e^+e^- \rightarrow WW$ measurement at CEPC using the methods described in Section 3.4. Both the results from the 240 GeV run alone and the ones from the combination of the 240 GeV and 350 GeV runs are shown.

FCC-ee								
	240 GeV(10 ab ⁻¹)				240 GeV(10 ab ⁻¹)+350 GeV(2.6 ab ⁻¹)			
	uncertainty	correlation matrix			uncertainty	correlation matrix		
		$\delta g_{1,Z}$	$\delta\kappa_\gamma$	λ_Z		$\delta g_{1,Z}$	$\delta\kappa_\gamma$	λ_Z
$\delta g_{1,Z}$	0.0064	1	0.066	-0.93	0.0029	1	-0.61	-0.88
$\delta\kappa_\gamma$	0.0034		1	-0.40	0.0014		1	0.19
λ_Z	0.0062			1	0.0022			1

Table 6: Same as Table 5 but for FCC-ee.

ILC (CLIC)				
	uncertainty	correlation matrix		
		$\delta g_{1,Z}$	$\delta\kappa_\gamma$	λ_Z
$\delta g_{1,Z}$	6.1×10^{-4}	1	0.634	0.477
$\delta\kappa_\gamma$	6.4×10^{-4}		1	0.354
λ_Z	7.2×10^{-4}			1

Table 7: The estimated statistical precision of aTGCs from the $e^+e^- \rightarrow WW$ measurements at ILC in Ref. [68], assuming 500 fb⁻¹ of data equally shared between four $P(e^-, e^+) = (\pm 0.8, \pm 0.3)$ beam polarization configurations at 500 GeV. We use the same results for CLIC. No scaling with statistics or center-of-mass energy is performed, given that systematic uncertainties may become important.

While δy_c is set to zero in obtaining these results (due to the fact that Ref. [73] did not provide estimations for the decay $h \rightarrow c\bar{c}$), it is not set to zero when the χ^2 is combined with the ones from future e^+e^- colliders. However, this has little impact on the results of the combined fits.

LHC 8 TeV Higgs + LEP $e^+e^- \rightarrow WW$											
	uncertainty	correlation matrix									
		δc_Z	c_{ZZ}	$c_{Z\Box}$	$c_{\gamma\gamma}$	$c_{Z\gamma}$	c_{gg}	δy_u	δy_d	δy_e	λ_Z
δc_Z	0.17	1	-0.04	-0.21	-0.76	-0.15	0.15	0.12	0.88	0.71	-0.22
c_{ZZ}	0.42		1	-0.96	0.37	0.19	0.03	0.04	-0.12	-0.31	-0.88
$c_{Z\Box}$	0.19			1	-0.17	-0.10	-0.07	-0.06	-0.10	0.12	0.93
$c_{\gamma\gamma}$	0.015				1	0.20	-0.12	-0.07	-0.79	-0.74	-0.13
$c_{Z\gamma}$	0.098					1	-0.01	-0.01	-0.15	-0.18	-0.10
c_{gg}	0.0027						1	-0.87	0.26	0.17	-0.07
δy_u	0.30							1	0.13	0.11	-0.06
δy_d	0.35								1	0.81	-0.11
δy_e	0.20									1	0.09
λ_Z	0.073										1

Table 8: Current constraints on the Higgs basis parameters from Ref. [23], obtained from the LHC 8 TeV Higgs measurements and LEP $e^+e^- \rightarrow WW$ measurements. Flavor universality is imposed. To transform it into our framework we simply take $\delta y_u \rightarrow \delta y_t$, $\delta y_d \rightarrow \delta y_b$, $\delta y_e \rightarrow \delta y_\tau$. For consistency we also set the central values to zero.

LHC 14 TeV Higgs measurements (300 fb $^{-1}$)											
	uncertainty	correlation matrix									
		δc_Z	c_{ZZ}	$c_{Z\Box}$	$c_{\gamma\gamma}$	$c_{Z\gamma}$	c_{gg}	δy_t	δy_b	δy_τ	δy_μ
δc_Z	0.116	1	-0.029	-0.037	-0.61	-0.29	0.037	0.36	0.88	0.50	0.43
c_{ZZ}	0.960		1	-0.996	0.77	0.52	-0.17	0.43	-0.21	-0.73	-0.55
$c_{Z\Box}$	0.419			1	-0.73	-0.50	0.17	-0.46	0.15	0.70	0.52
$c_{\gamma\gamma}$	0.0156				1	0.57	-0.18	0.13	-0.69	-0.85	-0.68
$c_{Z\gamma}$	0.0164					1	-0.10	0.070	-0.41	-0.54	-0.41
c_{gg}	0.00137						1	-0.74	0.063	0.14	0.26
δy_t	0.220							1	0.42	-0.094	-0.20
δy_b	0.303								1	0.61	0.47
δy_τ	0.196									1	0.60
δy_μ	0.271										1

Table 9: One sigma constraints and the correlation matrix of the Higgs basis parameters from the LHC 14 TeV Higgs measurements with 300 fb $^{-1}$ data, using the ATLAS projection with no theory error [73]. δy_c to set to zero since Ref. [73] did not provide estimations for the decay $h \rightarrow c\bar{c}$.

C Additional figures

Here we provide additional results of the global fits. In our study, conservative estimates have been made for the measurements of the diboson process ($e^+e^- \rightarrow WW$) which often end up being systematics dominated. To give a sense of the impact of these systematic uncertainties we show, in Fig. 13, global fit results in which aTGCs are assumed to be perfectly constrained.

Figure 14 reproduces the results in Fig. 7 in the basis defined by Eq. (A.8) and Table 1. The analogues to the figures presented in the main text for the CEPC, Fig. 8–12, are given here for the FCC-ee and ILC in Fig. 15–21. In particular, Fig. 16 shows the precision reach for ILC with different scenarios including runs at 250 GeV, 350 GeV and 500 GeV, while Fig. 17 further shows the potential improvement with the inclusion of a 1 TeV run.

LHC 14 TeV Higgs measurements (3000 fb ⁻¹)											
	uncertainty	correlation matrix									
		δc_Z	c_{ZZ}	$c_{Z\Box}$	$c_{\gamma\gamma}$	$c_{Z\gamma}$	c_{gg}	δy_t	δy_b	δy_τ	δy_μ
δc_Z	0.0500	1	0.0015	-0.045	-0.54	-0.22	0.034	0.38	0.87	0.40	0.45
c_{ZZ}	0.495		1	-0.998	0.81	0.46	-0.19	0.55	-0.22	-0.62	-0.68
$c_{Z\Box}$	0.214			1	-0.78	-0.44	0.20	-0.57	0.18	0.60	0.66
$c_{\gamma\gamma}$	0.00738				1	0.50	-0.20	0.27	-0.66	-0.73	-0.81
$c_{Z\gamma}$	0.00935					1	-0.099	0.13	-0.34	-0.39	-0.42
c_{gg}	0.000462						1	-0.65	0.086	0.13	0.26
δy_t	0.0856							1	0.39	-0.15	-0.30
δy_b	0.125								1	0.50	0.54
δy_τ	0.114									1	0.61
δy_μ	0.108										1

Table 10: Same as Table 9 but for 14 TeV LHC 3000 fb⁻¹. Note that while δy_c is set to zero in obtaining these results, it is not set to zero when the χ^2 is combined with the ones from future e^+e^- colliders. This has little impact on the results of the combined fits.

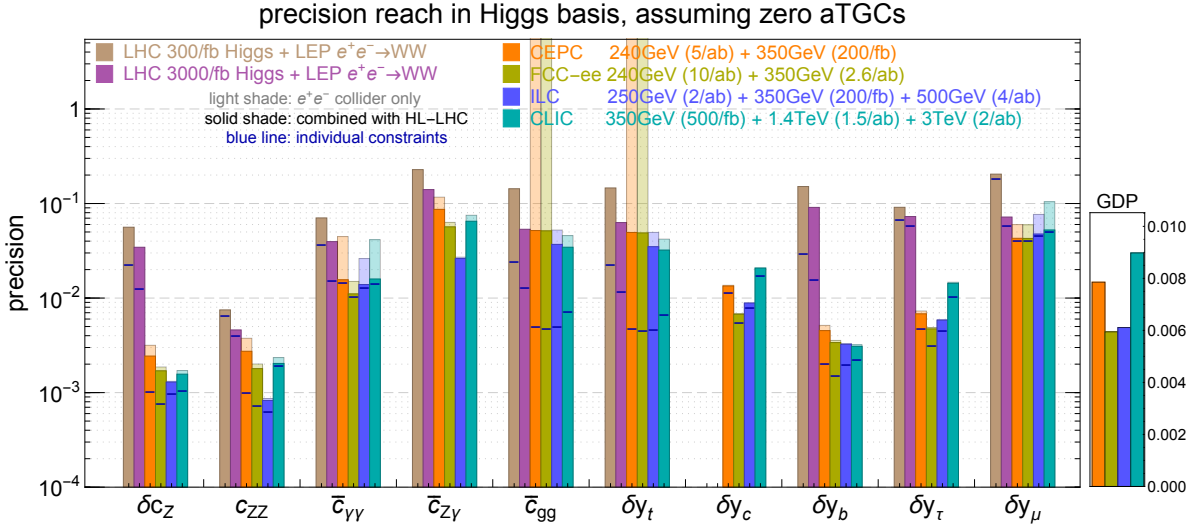


Figure 13: Same as Fig. 7 but assuming vanishing aTGCs. Imposing $\delta g_{1,Z} = \delta \kappa_\gamma = \lambda_Z = 0$, both λ_Z and $c_{Z\Box}$ are eliminated, while the relation $e^2 c_{\gamma\gamma} + (g^2 - g'^2) c_{Z\gamma} - (g^2 + g'^2) c_{ZZ} = 0$ is imposed among c_{ZZ} , $c_{\gamma\gamma}$ and $c_{Z\gamma}$. Note that the individual constraints are basis dependent. We use the above relation to eliminate $c_{Z\gamma}$, hence its individual constraints are not shown.

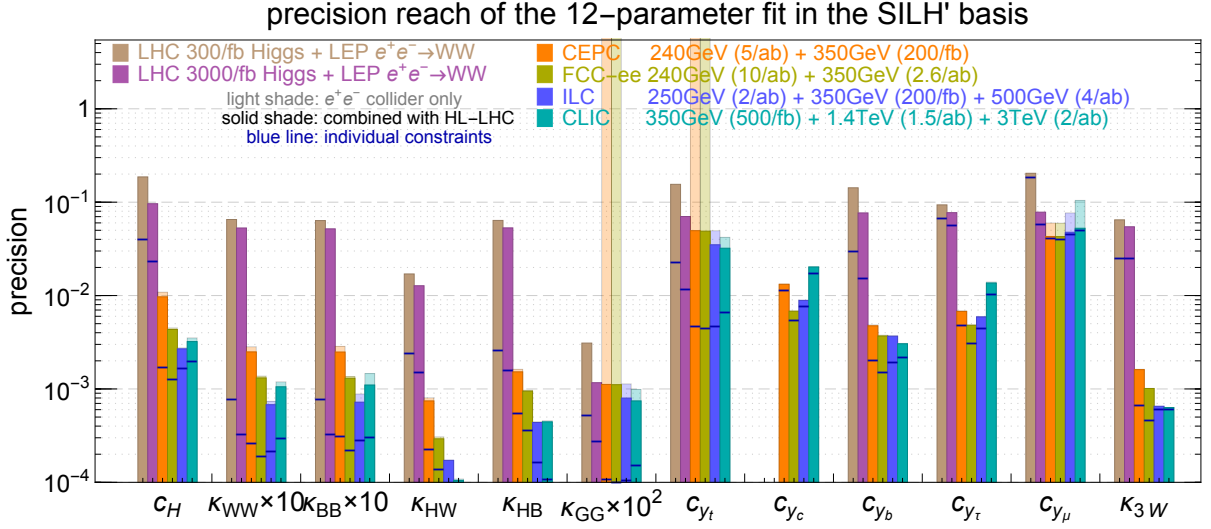


Figure 14: Same as Fig. 7 but is in the SILH'(-like) basis defined by Eq. (A.8) and Table 1.

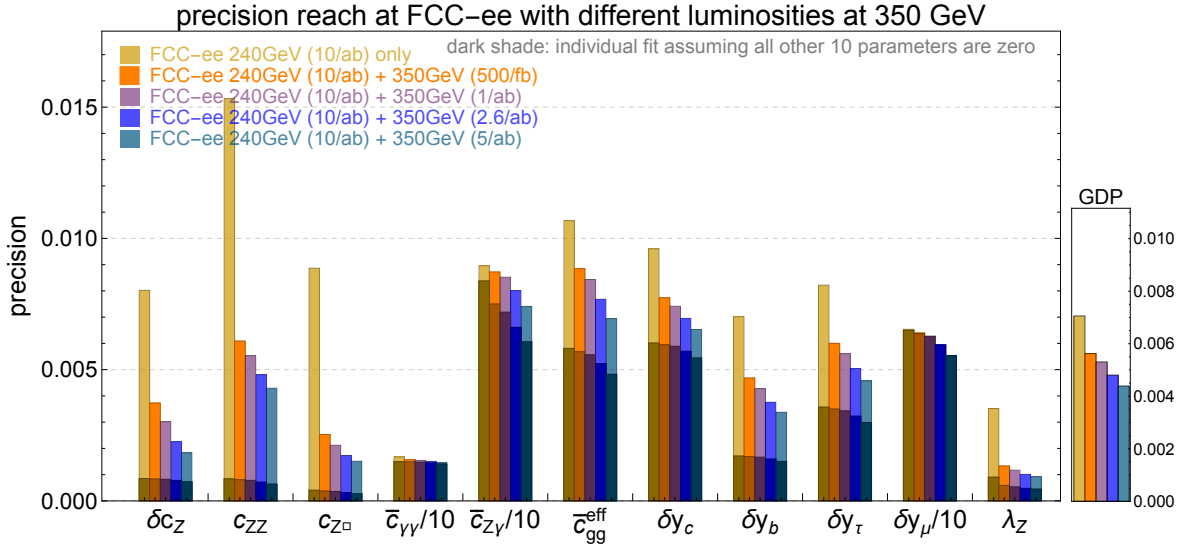


Figure 15: Same as Fig. 9 but for FCC-ee with 10 ab^{-1} at 240 GeV and 500 fb^{-1} , 1 ab^{-1} , 2.6 ab^{-1} and 5 ab^{-1} .

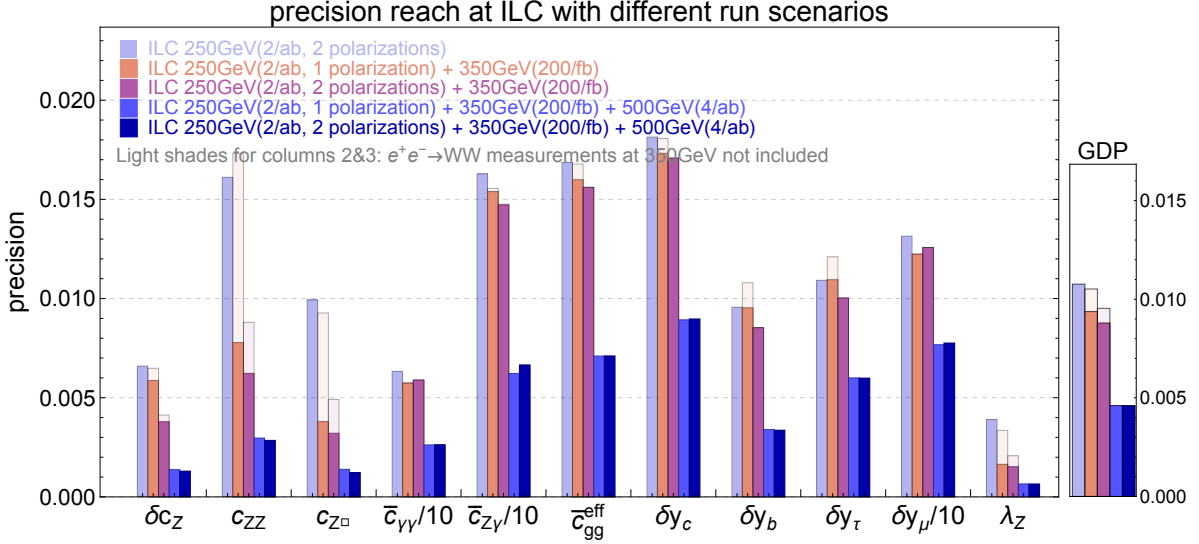


Figure 16: The precision reach for ILC with different scenarios. The 1st column corresponds to the ILC 250 GeV run with 2 ab^{-1} luminosity which is divided into two runs with polarizations $P(e^-, e^+) = (-0.8, +0.3)$ and $(+0.8, -0.3)$, and fractions 0.7 and 0.3, respectively (see Fig. 10). The 2nd and 3rd columns include ILC 250 GeV (2 ab^{-1}) and 350 GeV (200 fb^{-1}). For the 2nd column, only the $(-0.8, +0.3)$ polarization is used for the 240 GeV run, while for the 3rd column the 240 GeV run is divided in the same way as for the 1st column. The results of the ILC full run (2 ab^{-1} at 250 GeV, 200 fb^{-1} at 350 GeV and 4 ab^{-1} at 500 GeV) are shown in the 4th and 5th columns, while single polarization (two polarizations) at 250 GeV has been assumed for the 4th (5th) column, analogous to the 2nd and 3rd columns. $P(e^-, e^+) = (-0.8, +0.3)$ is assumed for the 350 GeV and 500 GeV runs. We found that dividing the runs at 350 GeV and 500 GeV into multiple polarization does not improve the results. For the ILC full program, we still show the constraint of $\bar{c}_{gg}^{\text{eff}}$ instead of c_{gg} and δy_t in order to compare with other scenarios. For the full program only the 500 GeV TGC results are used for consistency with the main results in Fig. 7.

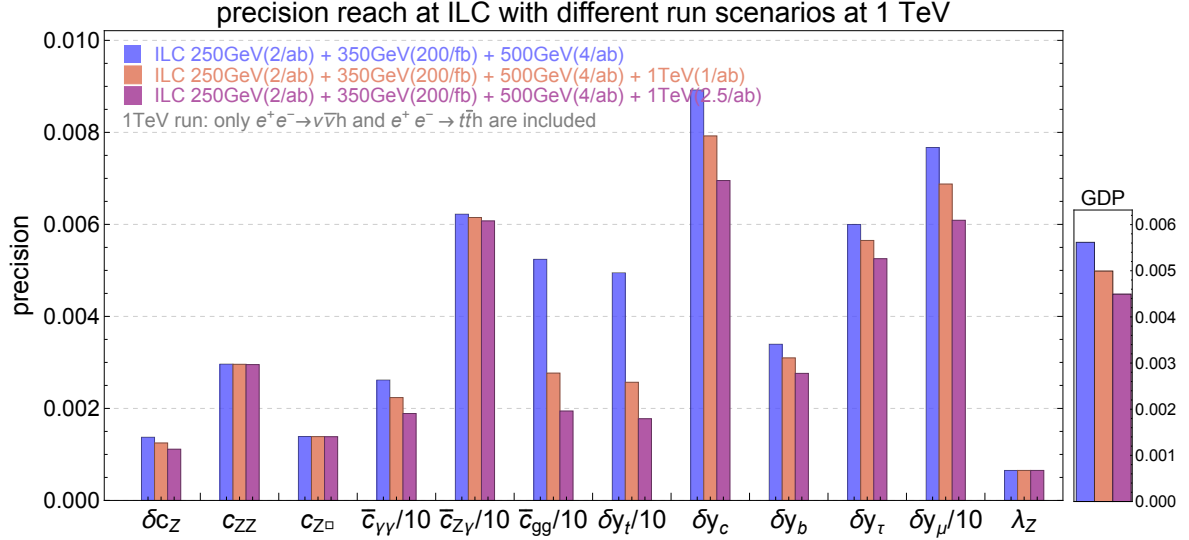


Figure 17: The precision reach for ILC with different scenarios for the 1 TeV run. The 1st column corresponds to the ILC full run considered in our study with 2 ab^{-1} at 250 GeV, 200 fb^{-1} at 350 GeV and 4 ab^{-1} at 500 GeV and a fixed polarization of $P(e^-, e^+) = (-0.8, +0.3)$. For the 2nd (3rd) column, an additional run at 1 TeV with an integrated luminosity of 1 ab^{-1} (2.5 ab^{-1}) and polarization $P(e^-, e^+) = (-0.8, +0.2)$ is also included. For the 1 TeV run, the estimated measurement precisions in Ref. [59] are used. Only the measurements of the $e^+e^- \rightarrow \nu\bar{\nu}h$ and $e^+e^- \rightarrow t\bar{t}h$ processes are included at 1 TeV, as the ones for $e^+e^- \rightarrow hZ$ and $e^+e^- \rightarrow WW$ are not provided. In particular, the precision of $\sigma(t\bar{t}h) \times \text{BR}(h \rightarrow b\bar{b})$ at 1 TeV is estimated to be 6.0% with 1 ab^{-1} data and 3.8% with 2.5 ab^{-1} data, which significantly improves the precision at 500 GeV. As such, the constraints on both \bar{c}_{gg} and δy_t are greatly improved. It should be noted that the $e^+e^- \rightarrow hZ$ and $e^+e^- \rightarrow WW$ processes are more sensitive to some of the EFT parameters at higher energies. The inclusion of their measurements could potentially further improve the overall reach of the global fit.

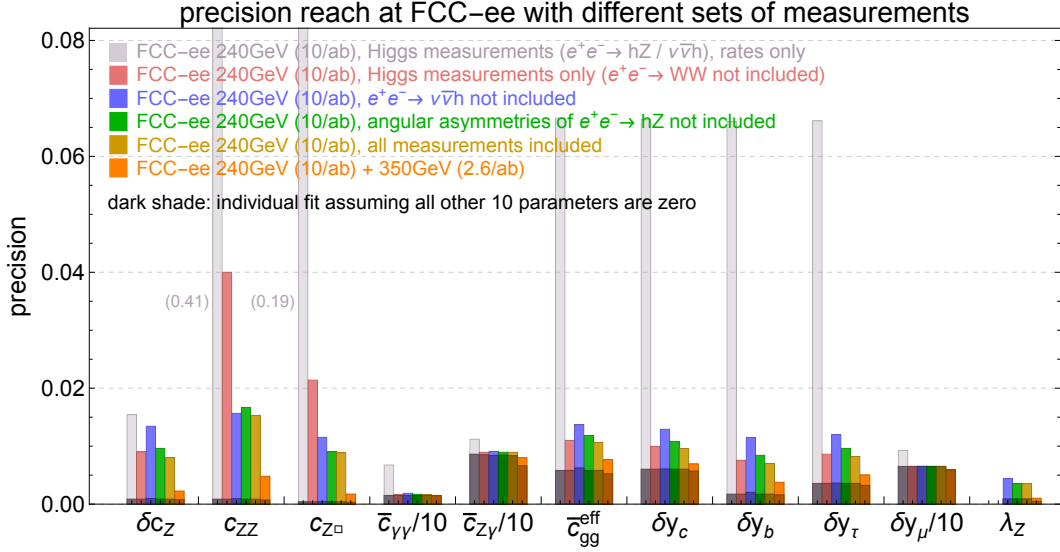


Figure 18: Same as Fig. 8 but for FCC-ee.

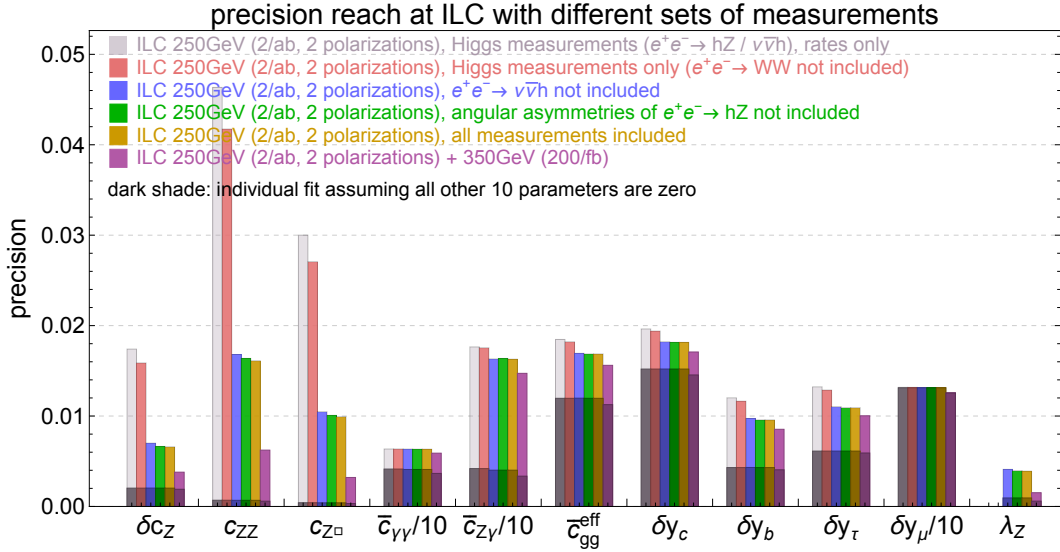


Figure 19: Same as Fig. 8 but for ILC with 2 ab^{-1} at 250 GeV and 200 fb^{-1} at 350 GeV. The 250 GeV run is divided into two runs with polarizations $P(e^-, e^+) = (-0.8, +0.3)$ and $(+0.8, -0.3)$, and fractions 0.7 and 0.3, respectively (see Fig. 10).

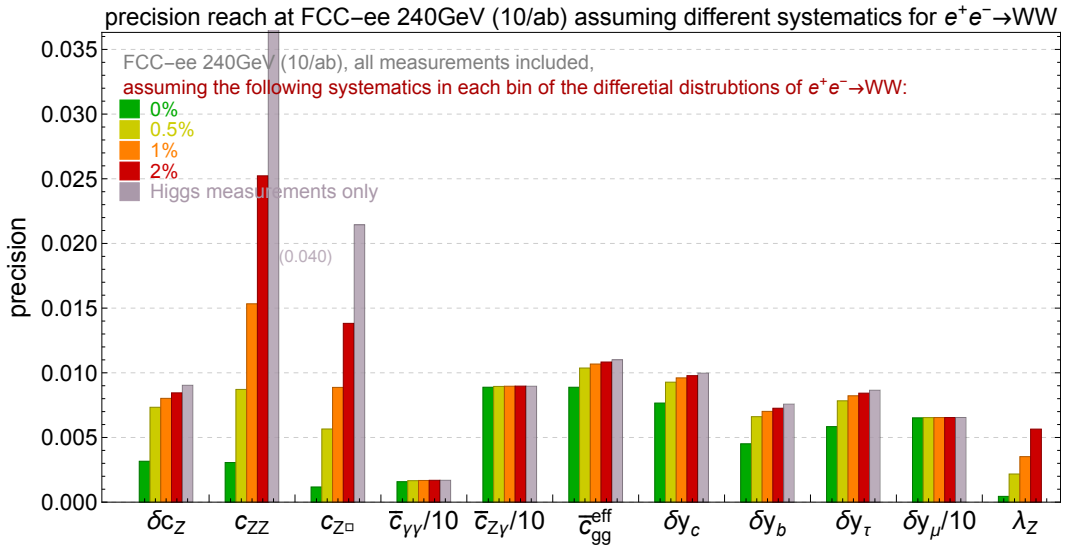
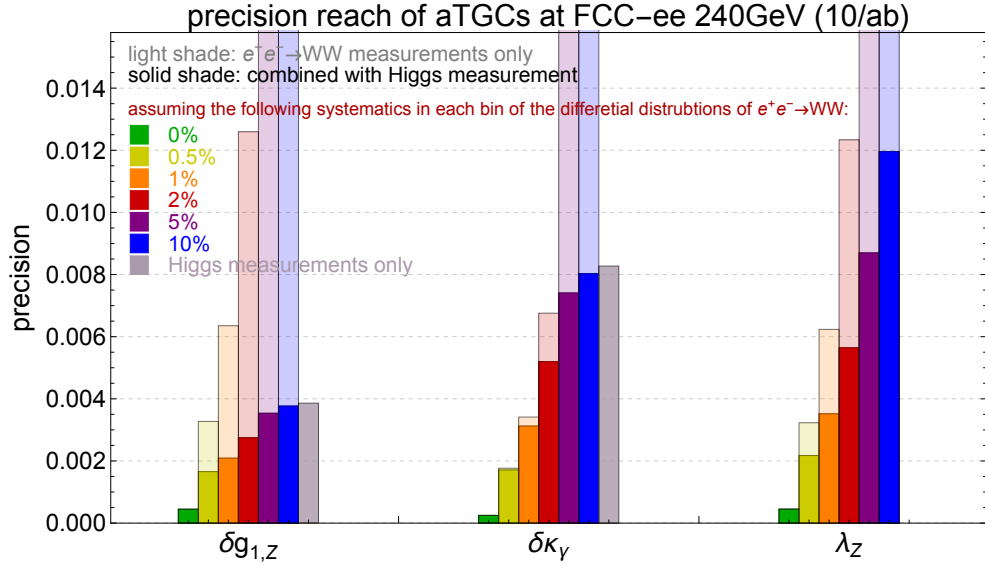


Figure 20: Same as Fig. 12 but for FCC-ee 240 GeV with 10 ab^{-1} .

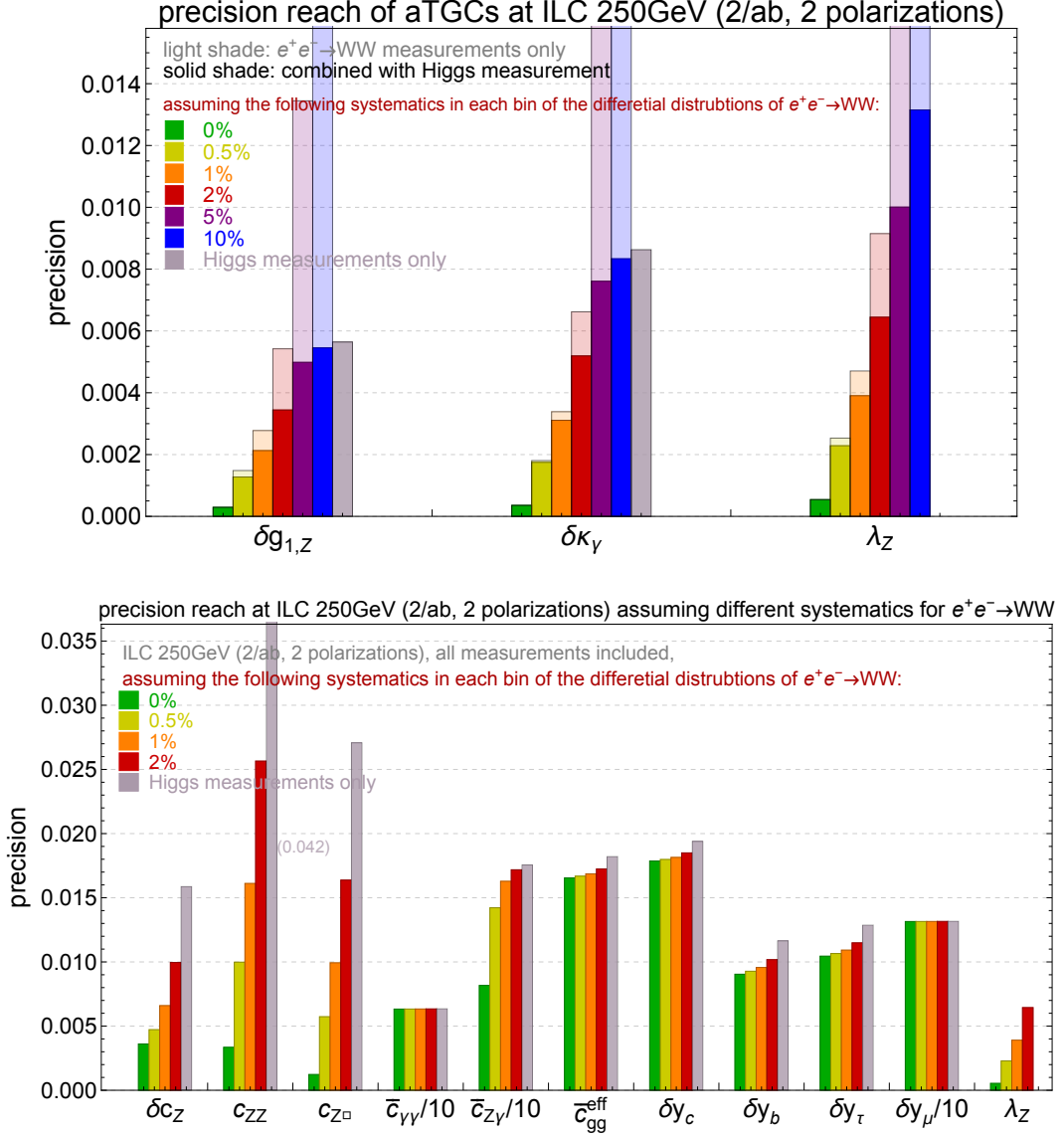


Figure 21: Same as Fig. 12 but for ILC 250 GeV with 2 ab^{-1} luminosity, divided into two runs with polarizations $P(e^-, e^+) = (-0.8, +0.3)$ and $(+0.8, -0.3)$, and fractions 0.7 and 0.3, respectively (see Fig. 10).

D Numerical expressions for the observables

We express some of the important observables as numerical functions of the parameters in Eq. (2.1), which is fed into the chi-square in Eq. (3.5)–Eq. (3.7). The SM input parameters we use in our analytical expressions are $G_F = 1.1663787 \times 10^{-5} \text{ GeV}^{-2}$, $m_Z = 91.1876 \text{ GeV}$, $\alpha_{\text{em}}(m_Z^2) = 1/127.940$ and $m_h = 125.09 \text{ GeV}$. For the rate of $e^+e^- \rightarrow hZ$, the measurements with the following energies and polarizations $P(e^-, e^+)$ are used,

$$\frac{\sigma_{hZ}}{\sigma_{hZ}^{\text{SM}}} \left| \begin{array}{l} 240 \text{ GeV unpolarized} \\ 250 \text{ GeV } (-0.8, +0.3) \\ 250 \text{ GeV } (+0.8, -0.3) \\ 350 \text{ GeV unpolarized} \\ 350 \text{ GeV } (-0.8, +0.3) \\ 500 \text{ GeV } (-0.8, +0.3) \\ 1.4 \text{ TeV unpolarized} \\ 3 \text{ TeV unpolarized} \end{array} \right. \simeq 1+2\delta c_{Z+} \begin{pmatrix} 1.8 \\ 5.6 \\ -2.9 \\ 2.8 \\ 11 \\ 21 \\ 14 \\ 52 \end{pmatrix} c_{ZZ+} \begin{pmatrix} 3.7 \\ 9.8 \\ -3.2 \\ 7.5 \\ 20 \\ 41 \\ 115 \\ 526 \end{pmatrix} c_{Z\Box+} \begin{pmatrix} -0.048 \\ -0.73 \\ 0.79 \\ -0.11 \\ -1.5 \\ -3.3 \\ -1.9 \\ -8.8 \end{pmatrix} c_{\gamma\gamma+} \begin{pmatrix} -0.087 \\ -1.3 \\ 1.5 \\ -0.24 \\ -3.3 \\ -8.1 \\ -5.5 \\ -26 \end{pmatrix} c_{Z\gamma}. \quad (\text{D.1})$$

As noted in Section 3.1, the interferences between s -channel Z and photon amplitudes are accidentally suppressed in the unpolarized total cross section. On the contrary, they have a significant impact when polarized beams are used, flipping for instance the sign of the c_{ZZ} prefactor as polarization is reversed at $\sqrt{s} = 250 \text{ GeV}$.¹¹ The relevant expressions for the WW fusion process are

$$\frac{\sigma_{WW \rightarrow h}}{\sigma_{WW \rightarrow h}^{\text{SM}}} \left| \begin{array}{l} 240 \text{ GeV} \\ 250 \text{ GeV} \\ 350 \text{ GeV} \\ 500 \text{ GeV} \\ 1 \text{ TeV} \\ 1.4 \text{ TeV} \\ 3 \text{ TeV} \end{array} \right. \simeq 1+2\delta c_{Z+} \begin{pmatrix} -0.25 \\ -0.27 \\ -0.40 \\ -0.53 \\ -0.76 \\ -0.86 \\ -1.1 \end{pmatrix} c_{ZZ+} \begin{pmatrix} -0.68 \\ -0.72 \\ -1.1 \\ -1.5 \\ -2.2 \\ -2.5 \\ -3.4 \end{pmatrix} c_{Z\Box+} \begin{pmatrix} 0.035 \\ 0.037 \\ 0.056 \\ 0.075 \\ 0.12 \\ 0.14 \\ 0.18 \end{pmatrix} c_{\gamma\gamma+} \begin{pmatrix} 0.090 \\ 0.097 \\ 0.14 \\ 0.20 \\ 0.32 \\ 0.37 \\ 0.52 \end{pmatrix} c_{Z\gamma}, \quad (\text{D.2})$$

which are obtained from `MadGraph5` [88] with the BSMC model [89, 90] as functions of δc_W , c_{WW} and $c_{W\Box}$ and then transformed into the basis in Eq. (2.1) with Eq. (A.3). The default input parameters are used for these numerical computations. They apply to any polarizations since only the initial states with helicities $H(e^-, e^+) = (-, +)$ contribute to this process.

For the $e^+e^- \rightarrow t\bar{t}h$ process, we only consider the dominate NP contribution which is from the modification of the top Yukawa, δy_t . It is therefore straight forward to write

¹¹For simplicity, the one-loop standard-model contributions to the $hZ\gamma$ vertex are not included in the expressions above. They have a relatively large impact on the numerical prefactors of the $c_{\gamma\gamma}$ and $c_{Z\gamma}$ coefficients which are accidentally suppressed in the unpolarized cross section, at 240 GeV in particular. Given that this measurement has little sensitivity to these coefficients, such contributions do however not affect the results of our global analysis. Note that the $c_{\gamma\Box}$ parameter, directly related to the $hZ\gamma$ vertex, is written in terms of c_{ZZ} , $c_{Z\Box}$, $c_{\gamma\gamma}$ and $c_{Z\gamma}$ using Eq. (A.3).

down the rate of the $t\bar{t}h$ process as

$$\frac{\sigma_{t\bar{t}h}}{\sigma_{t\bar{t}h}^{\text{SM}}} \simeq 1 + 2 \delta y_t. \quad (\text{D.3})$$

For Higgs decays, we make use of the results in Ref. [16]. The Decay widths to a pair of fermions are

$$\frac{\Gamma_{cc}}{\Gamma_{cc}^{\text{SM}}} \simeq 1 + 2 \delta y_c, \quad \frac{\Gamma_{bb}}{\Gamma_{bb}^{\text{SM}}} \simeq 1 + 2 \delta y_b, \quad \frac{\Gamma_{\tau\tau}}{\Gamma_{\tau\tau}^{\text{SM}}} \simeq 1 + 2 \delta y_\tau, \quad \frac{\Gamma_{\mu\mu}}{\Gamma_{\mu\mu}^{\text{SM}}} \simeq 1 + 2 \delta y_\mu. \quad (\text{D.4})$$

The decay width to $WW^* ZZ^*$ (with $4f$ final states) are given by

$$\frac{\Gamma_{WW^*}}{\Gamma_{WW^*}^{\text{SM}}} \simeq 1 + 2 \delta c_Z + 0.05 c_{ZZ} + 0.67 c_{Z\Box} - 0.05 c_{\gamma\gamma} - 0.17 c_{Z\gamma}, \quad (\text{D.5})$$

$$\frac{\Gamma_{ZZ^*}}{\Gamma_{ZZ^*}^{\text{SM}}} \simeq 1 + 2 \delta c_Z - 0.15 c_{ZZ} + 0.41 c_{Z\Box}, \quad (\text{D.6})$$

where we assume there is no NP correction to the gauge couplings of fermions. As stated in Section 2, we do not consider contribution from off-shell photons that gives the same final states as ZZ^* , as they can be relatively easily removed by kinematic cuts.

The decay of Higgs to gg , $\gamma\gamma$ and $Z\gamma$ are generated at one-loop level in the SM. The leading EFT contribution could either be at tree level (which are generated in the UV theory by new particles in the loop) or come at loop level by modifying the couplings in the SM loops. As mentioned in Section 2, we follow Ref. [16] and include both the tree level EFT contribution (c_{gg}) and the one-loop contribution (from δy_t and δy_b) for $h \rightarrow gg$, while only keeping the tree level EFT contribution ($c_{\gamma\gamma}$ and $c_{Z\gamma}$) for $h \rightarrow \gamma\gamma$ and $h \rightarrow Z\gamma$. The decay widths are given by ¹²

$$\frac{\Gamma_{gg}}{\Gamma_{gg}^{\text{SM}}} \simeq 1 + 241 c_{gg} + 2.10 \delta y_t - 0.10 \delta y_b, \quad (\text{D.7})$$

and

$$\begin{aligned} \frac{\Gamma_{\gamma\gamma}}{\Gamma_{\gamma\gamma}^{\text{SM}}} &\simeq \left(1 + \frac{c_{\gamma\gamma}}{-8.3 \times 10^{-2}}\right)^2, \\ \frac{\Gamma_{Z\gamma}}{\Gamma_{Z\gamma}^{\text{SM}}} &\simeq \left(1 + \frac{c_{Z\gamma}}{-5.9 \times 10^{-2}}\right)^2. \end{aligned} \quad (\text{D.8})$$

The branching ratio can be derived from the total decay width, which can be obtained from

$$\frac{\Gamma_{\text{tot}}}{\Gamma_{\text{tot}}^{\text{SM}}} = \sum_i \frac{\Gamma_i}{\Gamma_i^{\text{SM}}} \text{Br}_i^{\text{SM}}. \quad (\text{D.9})$$

¹²The choices of the bottom mass value would change the numerical values in Eq. (D.7), but has little impact on the global fit results.

In practice, one only needs to include the BSM effects of the main channels in the calculation of the total width. Finally, the physical observables in the form of $\sigma \times \text{BR}$ can be constructed from the above information.

For the aTGCs, we also express [Eq. \(A.6\)](#) numerically as

$$\begin{aligned}\delta g_{1,Z} &\simeq -0.120 c_{ZZ} - 0.392 c_{Z\Box} + 0.0215 c_{\gamma\gamma} + 0.0637 c_{Z\gamma}, \\ \delta \kappa_\gamma &\simeq 0.208 c_{ZZ} - 0.0373 c_{\gamma\gamma} - 0.11 c_{Z\gamma}.\end{aligned}\tag{D.10}$$

The expressions for the differential distributions in $e^+e^- \rightarrow WW$ for all energies and polarizations are too lengthy to be reported here. The necessary information can be conveniently reconstructed from the constraints on aTGCs in [Table 5](#), [6](#) and [7](#).

Finally, the CP-even angular observables in $e^+e^- \rightarrow hZ$ are given by

$$\begin{aligned}A_{\theta_1} &\simeq \begin{pmatrix} -0.45 \\ -0.46 \\ -0.46 \\ -0.57 \\ -0.57 \\ -0.65 \end{pmatrix} + \begin{pmatrix} 0.050 \\ 0.074 \\ 0.074 \\ 0.33 \\ 0.33 \\ 0.62 \end{pmatrix} c_{ZZ} + \begin{pmatrix} 0.0019 \\ 0.039 \\ -0.042 \\ 0.013 \\ 0.19 \\ 0.37 \end{pmatrix} c_{Z\gamma}, \\ A_\phi^{(3)} &\simeq \begin{pmatrix} 0.0093 \\ 0.069 \\ -0.065 \\ 0.0092 \\ 0.068 \\ 0.058 \end{pmatrix} + \begin{pmatrix} 0.32 \\ 0.059 \\ 0.10 \\ 0.75 \\ 0.15 \\ 0.34 \end{pmatrix} c_{ZZ} + \begin{pmatrix} 0.50 \\ 0.096 \\ 0.15 \\ 1.14 \\ 0.20 \\ 0.36 \end{pmatrix} c_{Z\Box} + \begin{pmatrix} -0.058 \\ -0.011 \\ -0.017 \\ -0.13 \\ -0.023 \\ -0.042 \end{pmatrix} c_{\gamma\gamma} + \begin{pmatrix} -0.11 \\ -0.023 \\ -0.034 \\ -0.28 \\ -0.036 \\ -0.025 \end{pmatrix} c_{Z\gamma}, \\ A_\phi^{(4)} &\simeq \begin{pmatrix} 0.096 \\ 0.092 \\ 0.092 \\ 0.061 \\ 0.061 \\ 0.035 \end{pmatrix} + \begin{pmatrix} 0.015 \\ 0.022 \\ 0.022 \\ 0.098 \\ 0.098 \\ 0.19 \end{pmatrix} c_{ZZ} + \begin{pmatrix} 0.00057 \\ 0.012 \\ -0.013 \\ 0.0040 \\ 0.056 \\ 0.11 \end{pmatrix} c_{Z\gamma}, \\ A_{c\theta_1, c\theta_2} &\simeq \begin{pmatrix} -0.0052 \\ -0.037 \\ 0.034 \\ -0.0033 \\ -0.024 \\ -0.014 \end{pmatrix} + \begin{pmatrix} -0.18 \\ -0.042 \\ -0.043 \\ -0.27 \\ -0.085 \\ -0.13 \end{pmatrix} c_{ZZ} + \begin{pmatrix} -0.28 \\ -0.050 \\ -0.078 \\ -0.40 \\ -0.070 \\ -0.086 \end{pmatrix} c_{Z\Box} + \begin{pmatrix} 0.032 \\ 0.0059 \\ 0.0092 \\ 0.047 \\ 0.0082 \\ 0.010 \end{pmatrix} c_{\gamma\gamma} + \begin{pmatrix} 0.054 \\ 0.0051 \\ 0.010 \\ 0.074 \\ -0.0092 \\ -0.028 \end{pmatrix} c_{Z\gamma},\end{aligned}\tag{D.11}$$

where the six entries in each column correspond to the center of energies and beam polarizations $P(e^-, e^+)$ in the following order: 240 GeV unpolarized, 250 GeV $(-0.8, +0.3)$, 250 GeV $(+0.8, -0.3)$, 350 GeV unpolarized, 350 GeV $(-0.8, +0.3)$ and 500 GeV $(-0.8, +0.3)$.

E Numerical results of the global fit

We hereby list the numerical results of the global fit for the future e^+e^- colliders. The one standard deviation constraints on each of the 12 parameters in Eq. (2.1) are listed in Table 11, and the corresponding correlation matrices are shown in Table 12–15. For each collider, the LHC 3000 fb^{-1} (including 8 TeV results) + LEP measurements are also combined in the total χ^2 , so that the results represent the “best reach” for each scenario. With this information, the corresponding chi-squared can be reconstructed using Eq. (3.8), which can be used to constrain any particular model that satisfies the assumptions of the 12-parameter framework, where the 12 parameters in EFT are functions of a usually much smaller set of model parameters. To minimize the numerical uncertainties, three significant figures are provided for the one standard deviation constraints, which is likely more than sufficient for the level of precision of our estimations. For easy mapping to dimension-6 operators and new physics models, we also switch back to the original definitions of $c_{\gamma\gamma}$, $c_{Z\gamma}$ and c_{gg} (instead of $\bar{c}_{\gamma\gamma}$, $\bar{c}_{Z\gamma}$ and \bar{c}_{gg}).

	precision (one standard deviation)			
	CEPC	FCC-ee	ILC	CLIC
δc_Z	0.00485	0.00216	0.00134	0.00161
c_{ZZ}	0.00701	0.00466	0.00291	0.00229
$c_{Z\Box}$	0.00328	0.00171	0.00139	0.000215
$c_{\gamma\gamma}$	0.00130	0.000922	0.00115	0.00132
$c_{Z\gamma}$	0.00537	0.00406	0.00332	0.00426
c_{gg}	0.000430	0.000427	0.000307	0.000286
δy_t	0.0495	0.0489	0.0349	0.0322
δy_c	0.0139	0.00686	0.00890	0.0208
δy_b	0.00559	0.00359	0.00334	0.00311
δy_τ	0.00769	0.00490	0.00592	0.0143
δy_μ	0.0429	0.0427	0.0476	0.0525
λ_Z	0.00161	0.00101	0.000652	0.000632

Table 11: Precision reach (one standard deviation bounds) at each of the four future e^+e^- colliders. For each collider, the LHC 3000 fb^{-1} (including 8 TeV results) + LEP measurements are also combined in the total χ^2 .

correlation matrix, CEPC

	δc_Z	c_{ZZ}	$c_{Z\Box}$	$c_{\gamma\gamma}$	$c_{Z\gamma}$	c_{gg}	δy_t	δy_c	δy_b	δy_τ	δy_μ	λ_Z
δc_Z	1	-0.37	-0.39	-0.072	-0.15	0.023	0.041	0.31	0.60	0.50	0.050	-0.21
c_{ZZ}		1	-0.69	0.083	0.34	-0.028	-0.015	-0.19	-0.44	-0.33	-0.040	-0.72
$c_{Z\Box}$			1	-0.0092	-0.18	0.0094	-0.022	-0.063	-0.11	-0.11	-0.0076	0.89
$c_{\gamma\gamma}$				1	0.028	-0.17	0.19	-0.049	-0.069	-0.063	-0.044	-0.016
$c_{Z\gamma}$					1	-0.014	-0.011	-0.11	-0.25	-0.18	-0.021	-0.11
c_{gg}						1	-0.99	0.014	0.035	0.025	0.16	0.011
δy_t							1	0.039	0.077	0.061	-0.16	-0.012
δy_c								1	0.48	0.37	0.036	-0.011
δy_b									1	0.76	0.067	-0.0012
δy_τ										1	0.054	-0.019
δy_μ											1	0.0017
λ_Z												1

Table 12: The corresponding correlation matrix for the CEPC one sigma bounds in Table 11.

correlation matrix, FCC-ee

	δc_Z	c_{ZZ}	$c_{Z\Box}$	$c_{\gamma\gamma}$	$c_{Z\gamma}$	c_{gg}	δy_t	δy_c	δy_b	δy_τ	δy_μ	λ_Z
δc_Z	1	-0.49	0.073	-0.055	-0.22	0.026	0.0056	0.19	0.26	0.26	0.013	0.17
c_{ZZ}		1	-0.88	0.13	0.34	-0.023	-0.0025	-0.24	-0.44	-0.33	-0.027	-0.81
$c_{Z\Box}$			1	-0.077	-0.20	0.013	-0.0018	0.13	0.24	0.15	0.015	0.86
$c_{\gamma\gamma}$				1	0.057	-0.13	0.13	-0.10	-0.16	-0.13	-0.034	-0.069
$c_{Z\gamma}$					1	-0.013	-0.0038	-0.15	-0.27	-0.20	-0.015	-0.081
c_{gg}						1	-0.99	0.026	0.049	0.036	0.16	0.012
δy_t							1	0.020	0.034	0.027	-0.16	0.0008
δy_c								1	0.55	0.43	0.023	0.13
δy_b									1	0.75	0.038	0.25
δy_τ										1	0.031	0.17
δy_μ											1	0.016
λ_Z												1

Table 13: The corresponding correlation matrix for the FCC-ee one sigma bounds in Table 11.

correlation matrix, ILC

	δc_Z	c_{ZZ}	$c_{Z\Box}$	$c_{\gamma\gamma}$	$c_{Z\gamma}$	c_{gg}	δy_t	δy_c	δy_b	δy_τ	δy_μ	λ_Z
δc_Z	1	-0.40	0.27	0.039	-0.26	0.020	0.0087	0.091	-0.059	0.13	-0.0085	-0.069
c_{ZZ}		1	-0.89	0.071	0.36	-0.027	0.0020	-0.13	-0.29	-0.24	-0.014	0.23
$c_{Z\Box}$			1	-0.020	0.08	0.019	-0.00026	0.087	0.22	0.15	0.0094	-0.25
$c_{\gamma\gamma}$				1	-0.024	-0.10	0.13	-0.030	-0.046	-0.043	-0.025	0.0061
$c_{Z\gamma}$					1	-0.0049	-0.013	-0.084	-0.17	-0.20	-0.0066	0.0096
c_{gg}						1	-0.98	0.029	0.081	0.046	0.12	-0.0049
δy_t							1	0.014	0.022	0.019	-0.13	-0.0000
δy_c								1	0.40	0.26	0.013	-0.023
δy_b									1	0.60	0.024	-0.058
δy_τ										1	0.019	-0.039
δy_μ											1	-0.0025
λ_Z												1

Table 14: The corresponding correlation matrix for the ILC one sigma bounds in Table 11.

correlation matrix, CLIC

	δc_Z	c_{ZZ}	$c_{Z\Box}$	$c_{\gamma\gamma}$	$c_{Z\gamma}$	c_{gg}	δy_t	δy_c	δy_b	δy_τ	δy_μ	λ_Z
δc_Z	1	-0.0065	-0.14	0.089	-0.17	0.088	0.048	0.36	0.30	0.49	-0.019	-0.013
c_{ZZ}		1	-0.46	0.051	0.73	-0.013	-0.0070	-0.054	-0.13	-0.083	-0.0014	-0.0083
$c_{Z\Box}$			1	0.022	0.14	-0.0014	0.0064	0.0027	-0.073	0.0050	-0.0054	0.020
$c_{\gamma\gamma}$				1	-0.023	-0.041	0.14	-0.032	0.013	-0.052	-0.043	0.0032
$c_{Z\gamma}$					1	-0.012	-0.015	-0.056	-0.22	-0.084	-0.0033	0.027
c_{gg}						1	-0.95	0.013	0.10	0.016	0.11	-0.0004
δy_t							1	0.023	0.035	0.031	-0.13	0.0005
δy_c								1	0.30	0.095	0.011	-0.0008
δy_b									1	0.42	0.0057	-0.0082
δy_τ										1	0.016	-0.0012
δy_μ											1	-0.0005
λ_Z												1

Table 15: The corresponding correlation matrix for the CLIC one sigma bounds in [Table 11](#).

References

- [1] CEPC-SPPC Study Group, *CEPC-SPPC Preliminary Conceptual Design Report. 1. Physics and Detector* (2015).
- [2] TLEP Design Study Working Group collaboration, M. Bicer et al., *First Look at the Physics Case of TLEP*, *JHEP* **01** (2014) 164, [[1308.6176](#)].
- [3] H. Baer, T. Barklow, K. Fujii, Y. Gao, A. Hoang, S. Kanemura et al., *The International Linear Collider Technical Design Report - Volume 2: Physics*, [[1306.6352](#)].
- [4] CLICdp, CLIC collaboration, M. J. Boland et al., *Updated baseline for a staged Compact Linear Collider*, [[1608.07537](#)].
- [5] LHC Higgs Cross Section Working Group collaboration, David, A. et al., *LHC HXSWG interim recommendations to explore the coupling structure of a Higgs-like particle*, [[1209.0040](#)].
- [6] W. Buchmuller and D. Wyler, *Effective Lagrangian Analysis of New Interactions and Flavor Conservation*, *Nucl. Phys.* **B268** (1986) 621–653.
- [7] G. F. Giudice, C. Grojean, A. Pomarol and R. Rattazzi, *The Strongly-Interacting Light Higgs*, *JHEP* **06** (2007) 045, [[hep-ph/0703164](#)].
- [8] B. Grzadkowski, M. Iskrzynski, M. Misiak and J. Rosiek, *Dimension-Six Terms in the Standard Model Lagrangian*, *JHEP* **10** (2010) 085, [[1008.4884](#)].
- [9] R. Contino, M. Ghezzi, C. Grojean, M. Muhlleitner and M. Spira, *Effective Lagrangian for a light Higgs-like scalar*, *JHEP* **07** (2013) 035, [[1303.3876](#)].
- [10] B. Henning, X. Lu and H. Murayama, *How to use the Standard Model effective field theory*, *JHEP* **01** (2016) 023, [[1412.1837](#)].
- [11] LHC Higgs Cross Section Working Group collaboration, D. de Florian et al., *Handbook of LHC Higgs Cross Sections: 4. Deciphering the Nature of the Higgs Sector*, [[1610.07922](#)].
- [12] A. Kobach, *Baryon Number, Lepton Number, and Operator Dimension in the Standard Model*, *Phys. Lett.* **B758** (2016) 455–457, [[1604.05726](#)].
- [13] J. Elias-Miro, J. R. Espinosa, E. Masso and A. Pomarol, *Higgs windows to new physics through $d=6$ operators: constraints and one-loop anomalous dimensions*, *JHEP* **11** (2013) 066, [[1308.1879](#)].
- [14] A. Pomarol and F. Riva, *Towards the Ultimate SM Fit to Close in on Higgs Physics*, *JHEP* **01** (2014) 151, [[1308.2803](#)].

- [15] J. Ellis, V. Sanz and T. You, *Complete Higgs Sector Constraints on Dimension-6 Operators*, *JHEP* **07** (2014) 036, [[1404.3667](#)].
- [16] A. Falkowski, *Effective field theory approach to LHC Higgs data*, *Pramana* **87** (2016) 39, [[1505.00046](#)].
- [17] A. Butter, O. J. P. Éboli, J. Gonzalez-Fraile, M. C. Gonzalez-Garcia, T. Plehn and M. Rauch, *The Gauge-Higgs Legacy of the LHC Run I*, *JHEP* **07** (2016) 152, [[1604.03105](#)].
- [18] Z. Han and W. Skiba, *Effective theory analysis of precision electroweak data*, *Phys. Rev.* **D71** (2005) 075009, [[hep-ph/0412166](#)].
- [19] M. Ciuchini, E. Franco, S. Mishima and L. Silvestrini, *Electroweak Precision Observables, New Physics and the Nature of a 126 GeV Higgs Boson*, *JHEP* **08** (2013) 106, [[1306.4644](#)].
- [20] M. Ciuchini, E. Franco, S. Mishima, M. Pierini, L. Reina and L. Silvestrini, *Update of the electroweak precision fit, interplay with Higgs-boson signal strengths and model-independent constraints on new physics*, *Nucl. Part. Phys. Proc.* **273-275** (2016) 2219–2225, [[1410.6940](#)].
- [21] A. Falkowski and F. Riva, *Model-independent precision constraints on dimension-6 operators*, *JHEP* **02** (2015) 039, [[1411.0669](#)].
- [22] A. Efrati, A. Falkowski and Y. Soreq, *Electroweak constraints on flavorful effective theories*, *JHEP* **07** (2015) 018, [[1503.07872](#)].
- [23] A. Falkowski, M. Gonzalez-Alonso, A. Greljo and D. Marzocca, *Global constraints on anomalous triple gauge couplings in effective field theory approach*, *Phys. Rev. Lett.* **116** (2016) 011801, [[1508.00581](#)].
- [24] A. Falkowski, M. Gonzalez-Alonso, A. Greljo, D. Marzocca and M. Son, *Anomalous Triple Gauge Couplings in the Effective Field Theory Approach at the LHC*, *JHEP* **02** (2017) 115, [[1609.06312](#)].
- [25] Z. Zhang, *Time to Go Beyond Triple-Gauge-Boson-Coupling Interpretation of W Pair Production*, *Phys. Rev. Lett.* **118** (2017) 011803, [[1610.01618](#)].
- [26] J. Ellis, V. Sanz and T. You, *The Effective Standard Model after LHC Run I*, *JHEP* **03** (2015) 157, [[1410.7703](#)].
- [27] L. Berthier and M. Trott, *Consistent constraints on the Standard Model Effective Field Theory*, *JHEP* **02** (2016) 069, [[1508.05060](#)].
- [28] N. Craig, M. Farina, M. McCullough and M. Perelstein, *Precision Higgsstrahlung as a Probe of New Physics*, *JHEP* **03** (2015) 146, [[1411.0676](#)].

- [29] M. Beneke, D. Boito and Y.-M. Wang, *Anomalous Higgs couplings in angular asymmetries of $H \rightarrow Z\ell^+\ell^-$ and $e^+e^- \rightarrow HZ$* , *JHEP* **11** (2014) 028, [[1406.1361](#)].
- [30] B. Henning, X. Lu and H. Murayama, *What do precision Higgs measurements buy us?*, [[1404.1058](#)].
- [31] N. Craig, J. Gu, Z. Liu and K. Wang, *Beyond Higgs Couplings: Probing the Higgs with Angular Observables at Future e^+e^- Colliders*, *JHEP* **03** (2016) 050, [[1512.06877](#)].
- [32] J. Ellis and T. You, *Sensitivities of Prospective Future $e+e-$ Colliders to Decoupled New Physics*, *JHEP* **03** (2016) 089, [[1510.04561](#)].
- [33] S.-F. Ge, H.-J. He and R.-Q. Xiao, *Probing new physics scales from Higgs and electroweak observables at e^+e^- Higgs factory*, *JHEP* **10** (2016) 007, [[1603.03385](#)].
- [34] J. de Blas, M. Ciuchini, E. Franco, S. Mishima, M. Pierini, L. Reina et al., *Electroweak precision observables and Higgs-boson signal strengths in the Standard Model and beyond: present and future*, *JHEP* **12** (2016) 135, [[1608.01509](#)].
- [35] J. Ellis, P. Roloff, V. Sanz and T. You, *Dimension-6 Operator Analysis of the CLIC Sensitivity to New Physics*, *JHEP* **05** (2017) 096, [[1701.04804](#)].
- [36] H. Khanpour and M. Mohammadi Najafabadi, *Constraining Higgs boson effective couplings at electron-positron colliders*, *Phys. Rev.* **D95** (2017) 055026, [[1702.00951](#)].
- [37] D. Atwood and A. Soni, *Analysis for magnetic moment and electric dipole moment form-factors of the top quark via $e^+e^- \rightarrow t\bar{t}$* , *Phys. Rev.* **D45** (1992) 2405–2413.
- [38] M. Diehl and O. Nachtmann, *Optimal observables for the measurement of three gauge boson couplings in $e^+e^- \rightarrow W^+W^-$* , *Z. Phys.* **C62** (1994) 397–412.
- [39] A. Falkowski, *Higgs Basis: Proposal for an EFT basis choice for LHC HXSWG, LHCHSWG-INT-2015-001* (March, 2015).
- [40] S. M. Barr and A. Zee, *Electric Dipole Moment of the Electron and of the Neutron*, *Phys. Rev. Lett.* **65** (1990) 21–24.
- [41] J. Fan and M. Reece, *Probing Charged Matter Through Higgs Diphoton Decay, Gamma Ray Lines, and EDMs*, *JHEP* **06** (2013) 004, [[1301.2597](#)].
- [42] ACME collaboration, J. Baron et al., *Order of Magnitude Smaller Limit on the Electric Dipole Moment of the Electron*, *Science* **343** (2014) 269–272, [[1310.7534](#)].
- [43] Y. T. Chien, V. Cirigliano, W. Dekens, J. de Vries and E. Mereghetti, *Direct and indirect constraints on CP-violating Higgs-quark and Higgs-gluon interactions*, *JHEP* **02** (2016) 011, [[1510.00725](#)].

- [44] R. Harnik, A. Martin, T. Okui, R. Primulando and F. Yu, *Measuring CP violation in $h \rightarrow \tau^+\tau^-$ at colliders*, *Phys. Rev.* **D88** (2013) 076009, [[1308.1094](#)].
- [45] A. Azatov, R. Contino, C. S. Machado and F. Riva, *Helicity selection rules and noninterference for BSM amplitudes*, *Phys. Rev.* **D95** (2017) 065014, [[1607.05236](#)].
- [46] F. Goertz, *Indirect Handle on the Down-Quark Yukawa Coupling*, *Phys. Rev. Lett.* **113** (2014) 261803, [[1406.0102](#)].
- [47] W. Altmannshofer, J. Brod and M. Schmaltz, *Experimental constraints on the coupling of the Higgs boson to electrons*, *JHEP* **05** (2015) 125, [[1503.04830](#)].
- [48] A. L. Kagan, G. Perez, F. Petriello, Y. Soreq, S. Stoynev and J. Zupan, *Exclusive Window onto Higgs Yukawa Couplings*, *Phys. Rev. Lett.* **114** (2015) 101802, [[1406.1722](#)].
- [49] C. Hartmann and M. Trott, *Higgs Decay to Two Photons at One Loop in the Standard Model Effective Field Theory*, *Phys. Rev. Lett.* **115** (2015) 191801, [[1507.03568](#)].
- [50] S. Di Vita, C. Grojean, G. Panico, M. Riembau and T. Vantalon, *A global view on the Higgs self-coupling*, [[1704.01953](#)].
- [51] M. McCullough, *An Indirect Model-Dependent Probe of the Higgs Self-Coupling*, *Phys. Rev.* **D90** (2014) 015001, [[1312.3322](#)].
- [52] Y. Chen, R. Harnik and R. Vega-Morales, *New opportunities in $h \rightarrow 4\ell$* , *JHEP* **09** (2015) 185, [[1503.05855](#)].
- [53] S. Boselli, C. M. Carloni Calame, G. Montagna, O. Nicrosini, F. Piccinini and A. Shivaji, *Higgs decay into four charged leptons in the presence of dimension-six operators*, [[1703.06667](#)].
- [54] Z. Liu, L.-T. Wang and H. Zhang, *Exotic decays of the 125 GeV Higgs boson at future e^+e^- lepton colliders*, *Chin. Phys.* **C41** (2017) 063102, [[1612.09284](#)].
- [55] M. Ruan, “Status & Updates from CEPC.” https://indico.cern.ch/event/550509/contributions/2413240/attachments/1395641/2128022/CEPC_FCC_WS_v2.pdf, 2017.
- [56] M. Benedikt and F. Zimmermann, “Future Circular Collider Study, Status and Progress.” https://indico.cern.ch/event/550509/contributions/2413230/attachments/1396002/2128079/170116-MBE-FCC-Study-Status_ap.pdf, 2017.
- [57] K. Fujii et al., *Physics Case for the International Linear Collider*, [[1506.05992](#)].
- [58] T. Barklow, J. Brau, K. Fujii, J. Gao, J. List, N. Walker et al., *ILC Operating Scenarios*, [[1506.07830](#)].

- [59] D. M. Asner et al., *ILC Higgs White Paper*, in *Proceedings, Community Summer Study 2013: Snowmass on the Mississippi (CSS2013): Minneapolis, MN, USA, July 29-August 6, 2013*, 2013. [1310.0763](#).
- [60] H. Abramowicz et al., *Higgs physics at the CLIC electron-positron linear collider*, *Eur. Phys. J.* **C77** (2017) 475, [[1608.07538](#)].
- [61] D. R. T. Jones and S. T. Petcov, *Heavy Higgs Bosons at LEP*, *Phys. Lett.* **84B** (1979) 440–444.
- [62] P. S. Bhupal Dev, A. Djouadi, R. M. Godbole, M. M. Muhlleitner and S. D. Rindani, *Determining the CP properties of the Higgs boson*, *Phys. Rev. Lett.* **100** (2008) 051801, [[0707.2878](#)].
- [63] K. Hagiwara, S. Ishihara, R. Szalapski and D. Zeppenfeld, *Low-energy effects of new interactions in the electroweak boson sector*, *Phys. Rev.* **D48** (1993) 2182–2203.
- [64] G. Gounaris et al., *Triple gauge boson couplings*, in *AGS / RHIC Users Annual Meeting Upton, New York, June 15-16, 1995*, pp. 525–576, 1996. [hep-ph/9601233](#).
- [65] DELPHI, OPAL, LEP Electroweak, ALEPH, L3 collaboration, S. Schael et al., *Electroweak Measurements in Electron-Positron Collisions at W-Boson-Pair Energies at LEP*, *Phys. Rept.* **532** (2013) 119–244, [[1302.3415](#)].
- [66] Linear Collider American Working Group collaboration, T. Abe et al., *Linear Collider Physics Resource Book for Snowmass 2001 - Part 3: Studies of Exotic and Standard Model Physics*, [[hep-ex/0106057](#)].
- [67] CLIC Physics Working Group collaboration, E. Accomando et al., *Physics at the CLIC multi-TeV linear collider*, in *Proceedings, 11th International Conference on Hadron spectroscopy (Hadron 2005): Rio de Janeiro, Brazil, August 21-26, 2005*, 2004. [hep-ph/0412251](#).
- [68] I. Marchesini, *Triple gauge couplings and polarization at the ILC and leakage in a highly granular calorimeter*, *PhD thesis, Hamburg U.* (2011).
- [69] A. Rosca, *Measurement of the charged triple gauge boson couplings at the ILC*, *Nucl. Part. Phys. Proc.* **273-275** (2016) 2226–2231.
- [70] J. D. Wells and Z. Zhang, *Status and prospects of precision analyses with $e^+e^- \rightarrow W^+W^-$* , *Phys. Rev.* **D93** (2016) 034001, [[1507.01594](#)].
- [71] L. Bian, J. Shu and Y. Zhang, *Prospects for Triple Gauge Coupling Measurements at Future Lepton Colliders and the 14 TeV LHC*, *JHEP* **09** (2015) 206, [[1507.02238](#)].
- [72] J. List, *Private communications* (Aug, 2017).

- [73] *Projections for measurements of Higgs boson signal strengths and coupling parameters with the ATLAS detector at a HL-LHC*, [ATL-PHYS-PUB-2014-016](#) (Oct, 2014).
- [74] *Projections for measurements of Higgs boson cross sections, branching ratios and coupling parameters with the ATLAS detector at a HL-LHC*, [ATL-PHYS-PUB-2013-014](#) (Oct, 2013).
- [75] *HL-LHC projections for signal and background yield measurements of the $H \rightarrow \gamma\gamma$ when the Higgs boson is produced in association with t quarks, W or Z bosons*, [ATL-PHYS-PUB-2014-012](#) (Jul, 2014).
- [76] *Update of the prospects for the $H \rightarrow Z\gamma$ search at the High-Luminosity LHC*, [ATL-PHYS-PUB-2014-006](#) (May, 2014).
- [77] *Prospects for the study of the Higgs boson in the $VH(bb)$ channel at HL-LHC*, [ATL-PHYS-PUB-2014-011](#) (Jul, 2014).
- [78] *Studies of the VBF $H \rightarrow \tau_l\tau_{had}$ analysis at High Luminosity LHC conditions*, [ATL-PHYS-PUB-2014-018](#) (Oct, 2014).
- [79] R. Contino, A. Falkowski, F. Goertz, C. Grojean and F. Riva, *On the Validity of the Effective Field Theory Approach to SM Precision Tests*, [JHEP](#) **07** (2016) 144, [[1604.06444](#)].
- [80] ATLAS collaboration, *Search for the Standard Model Higgs and Z Boson decays to $J/\psi\gamma$: HL-LHC projections*, [ATL-PHYS-PUB-2015-043](#) (Sep, 2015).
- [81] G. T. Bodwin, F. Petriello, S. Stoynev and M. Velasco, *Higgs boson decays to quarkonia and the $H\bar{c}c$ coupling*, [Phys. Rev.](#) **D88** (2013) 053003, [[1306.5770](#)].
- [82] G. Perez, Y. Soreq, E. Stamou and K. Tobioka, *Constraining the charm Yukawa and Higgs-quark coupling universality*, [Phys. Rev.](#) **D92** (2015) 033016, [[1503.00290](#)].
- [83] I. Brivio, F. Goertz and G. Isidori, *Probing the Charm Quark Yukawa Coupling in Higgs+Charm Production*, [Phys. Rev. Lett.](#) **115** (2015) 211801, [[1507.02916](#)].
- [84] F. Bishara, U. Haisch, P. F. Monni and E. Re, *Constraining Light-Quark Yukawa Couplings from Higgs Distributions*, [Phys. Rev. Lett.](#) **118** (2017) 121801, [[1606.09253](#)].
- [85] L. M. Carpenter, T. Han, K. Hendricks, Z. Qian and N. Zhou, *Higgs Boson Decay to Light Jets at the LHC*, [Phys. Rev.](#) **D95** (2017) 053003, [[1611.05463](#)].
- [86] M. Ruan, “Status & Updates from CEPC Simulation -Detector optimization.” http://ias.ust.hk/program/shared_doc/2017/201701hep/HEP_20170124_Manqi_Ruan.pdf, 2017.

- [87] T. Han, Z. Liu, Z. Qian and J. Sayre, *Improving Higgs coupling measurements through ZZ Fusion at the ILC*, *Phys. Rev.* **D91** (2015) 113007, [[1504.01399](#)].
- [88] J. Alwall, R. Frederix, S. Frixione, V. Hirschi, F. Maltoni, O. Mattelaer et al., *The automated computation of tree-level and next-to-leading order differential cross sections, and their matching to parton shower simulations*, *JHEP* **07** (2014) 079, [[1405.0301](#)].
- [89] B. Fuks and K. Mawatari, “The BSM Characterisation model.” <http://feynrules.irmp.ucl.ac.be/wiki/BSMCharacterisation>, 2015.
- [90] A. Falkowski, B. Fuks, K. Mawatari, K. Mimasu, F. Riva and V. Sanz, *Rosetta: an operator basis translator for Standard Model effective field theory*, *Eur. Phys. J.* **C75** (2015) 583, [[1508.05895](#)].